NASA/CR–2013-218005

Large Civil Tiltrotor (LCTR2) Interior Noise Predictions Due to Turbulent Boundary Layer Excitation

Ferdinand W. Grosveld
Northrop Grumman, Langley Research Center, Hampton, Virginia

June 2013

NASA STI Program . . . in Profile

Since its founding, NASA has been dedicated to the advancement of aeronautics and space science. The NASA scientific and technical information (STI) program plays a key part in helping NASA maintain this important role.

The NASA STI program operates under the auspices of the Agency Chief Information Officer. It collects, organizes, provides for archiving, and disseminates NASA's STI. The NASA STI program provides access to the NASA Aeronautics and Space Database and its public interface, the NASA Technical Report Server, thus providing one of the largest collections of aeronautical and space science STI in the world. Results are published in both non-NASA channels and by NASA in the NASA STI Report Series, which includes the following report types:

- TECHNICAL PUBLICATION. Reports of completed research or a major significant phase of research that present the results of NASA Programs and include extensive data or theoretical analysis. Includes compilations of significant scientific and technical data and information deemed to be of continuing reference value. NASA counterpart of peer-reviewed formal professional papers, but having less stringent limitations on manuscript length and extent of graphic presentations.

- TECHNICAL MEMORANDUM. Scientific and technical findings that are preliminary or of specialized interest, e.g., quick release reports, working papers, and bibliographies that contain minimal annotation. Does not contain extensive analysis.

- CONTRACTOR REPORT. Scientific and technical findings by NASA-sponsored contractors and grantees.

- CONFERENCE PUBLICATION. Collected papers from scientific and technical conferences, symposia, seminars, or other meetings sponsored or co-sponsored by NASA.

- SPECIAL PUBLICATION. Scientific, technical, or historical information from NASA programs, projects, and missions, often concerned with subjects having substantial public interest.

- TECHNICAL TRANSLATION. English-language translations of foreign scientific and technical material pertinent to NASA's mission.

Specialized services also include organizing and publishing research results, distributing specialized research announcements and feeds, providing information desk and personal search support, and enabling data exchange services.

For more information about the NASA STI program, see the following:

- Access the NASA STI program home page at *http://www.sti.nasa.gov*

- E-mail your question to help@sti.nasa.gov

- Fax your question to the NASA STI Information Desk at 443-757-5803

- Phone the NASA STI Information Desk at 443-757-5802

- Write to:
  STI Information Desk
  NASA Center for AeroSpace Information
  7115 Standard Drive
  Hanover, MD 21076-1320

NASA/CR–2013-218005

Large Civil Tiltrotor (LCTR2) Interior Noise Predictions Due to Turbulent Boundary Layer Excitation

Ferdinand W. Grosveld
Northrop Grumman, Langley Research Center, Hampton, Virginia

National Aeronautics and
Space Administration

Langley Research Center
Hampton, Virginia 23681-2199

Prepared for Langley Research Center
under Contract NNL12AA09C

June 2013

Available from:

NASA Center for AeroSpace Information
7115 Standard Drive
Hanover, MD 21076-1320
443-757-5802

TABLE OF CONTENTS

LIST OF TABLES

LIST OF FIGURES

INTRODUCTION

The Large Civil Tiltrotor (LCTR) is a conceptual vehicle that was developed under the NASA Heavy Lift Systems Investigation[1] as an economically competitive alternative to medium range regional airliners that could significantly relieve runway and terminal area congestion. The tiltrotor design combines the speed, altitude and range of a turboprop airplane with the vertical lift capability of a helicopter thereby freeing up existing runways for use by larger and longer-range aircraft. A second-generation configuration of this vehicle, designated LCTR2 (Figure 1), has a design goal to transport ninety passengers over a distance of 1800 km at a speed of 556 km/hr. The LCTR2 was used as a representative vehicle design and mission under the NASA Fundamental Aeronautics Program (FAP) Subsonic Rotary Wing (SRW) project.[2,3] Several high risk areas have been identified for the LCTR2 configuration, such as the need for a high torque, low weight drive system and a high performance, structurally efficient rotor/wing system. Interior noise is expected to be distinctive due to the very low blade passage frequency of the four-bladed rotor (as low as 6.75 Hz during cruise conditions), the presence of a mid-wing gearbox and the turbulent boundary layer excitation during cruise flight conditions. When combined with the anticipated use of lightweight composite and sandwich materials in the fuselage sidewall, achieving acceptable interior noise levels in the LCTR2 will be challenging.

Previous efforts[4] to predict the interior noise environment focused on the transmission loss characteristics of a notional LCTR2 sidewall structure. The materials and lay-up of this hypothetical sidewall were chosen to be similar to a Bombardier Dash-8 Q400 fuselage section[5] for which limited interior noise measurement data are available in the literature.[6] The objective of the present study is to perform a preliminary assessment of the interior noise environment in the LCTR2 with this notional sidewall due to turbulent boundary layer excitation during cruise conditions. The analysis frequency of interest extends from 6 Hz through 8000 Hz. Interior noise due to thickness and loading noise from the rotating blades and mechanical noise radiated by the mid-wing gearbox will be the subjects of a future investigation.

VEHICLE DESCRIPTION

Isometric, top, front and side views of the ninety passenger second-generation LCTR2 design are presented in Figure 1, while an artist's rendering of the LCTR2 concept vehicle in forward flight is shown in Figure 2. Cruise operating altitude of the vehicle is 8,534 m. Each of the two tiltrotors has four blades with tip speeds of 107 m/s and helical tip Mach numbers of 0.61 during cruise. The rotational speed of approximately 102 rotations per minute (rpm) yields a blade passage frequency of 6.75 Hz. The design parameters for the LCTR2 are listed in Table 1.

CABIN DESIGN

The LCTR2 is a conceptual design and no details of the fuselage sidewall, materials, cabin arrangement, overhead bins or interior trim have yet been established. To enable preliminary assessment of the interior noise for this study, the notional fuselage construction and geometry, including the skin, the ring frames, longitudinal stringers, bulkheads, floor, floor support beams, sidewall trim panels and noise control/thermal protection treatment were chosen with dimensions and material properties typical for an aircraft of that size and range, such as a proposed stretched

90-passenger seating variant of the Bombardier Dash-8 Q400.[7] A hypothetical layout of the LCTR2 fuselage including seats, seat pitch, lavatory, galley, and baggage areas is sketched in Figure 3. The passenger cabin is 2.68 m in diameter and is assumed to start at the door to the flight deck, 3.66 m from the nose of the vehicle, and end at the aft bulkhead for a total length of 22.04 m. A notional cross-section of the LCTR2 passenger cabin is presented in Figure 4 showing four-abreast seating and two overhead bins. The maximum height in the cabin is 1.95 m. The nominal seat pitch is 0.79 m and the aisle was designed to be 0.40 m wide.

PREDICTION SCHEME

A prediction scheme was established to compute sound pressure levels in the interior of a simplified cabin model of the LCTR2, while being excited by a turbulent boundary layer flow over the fuselage. Structural and acoustic finite element models were created in MSC Patran 2012 64-bit[8] and the finite element geometries were imported into the VA One[9] vibro-acoustic analysis program. The fuselage structure, the cabin acoustic space and the cabin interior poro-elastic components were modeled in VA One as energy transmitting, storing and receiving vibro-acoustic systems. The external turbulent boundary excitation was represented as a fluctuating pressure spectrum consistent with semi-empirical turbulent boundary layer excitation predictions. The properties of the turbulent boundary layer were specified at nineteen axial sections of the fuselage structure to capture the evolution of the excitation in the flow direction as the boundary layer thickness changes. The sound pressure levels in the cabin were predicted employing different approaches for the low frequencies, 6-141 Hz with a 1 Hz analysis bandwidth, and the high frequency 125-8000 Hz one-third octave bands. The 141 Hz is the limiting frequency in the 125 Hz one-third octave band allowing comparison between the low and high frequency analyses in the overlapping 125 Hz one-third octave band.

At low frequencies, where acoustic and structural wavelengths are long compared to the dimensions of the sidewall structure and interior cabin, the vibro-acoustic response is deterministic and can be described by modal interactions between the structure and the interior acoustic space. Representative finite element models require a minimum of 4-6 elements per wavelength to produce accurate results and, consequently, their mesh densities define the upper frequency limit for the low frequency analysis. A modal analysis of the fuselage structure was performed in MSC Nastran[10] and the modal parameters and the mode shape deflection information were imported into the VA One program. Rigid-boundary acoustic modes were computed in VA One and were coupled with the in-vacuo modes of the structure by velocity continuity boundary conditions at their interfaces. Although the structural components and the acoustic space are modeled using finite elements, it is computationally efficient to use a stochastic representation for the sound radiated outward from the fuselage into the surrounding fluid. This is accomplished within VA One by using a hybrid method,[9] which combines Finite Elements (FE) with Statistical Energy Analysis (SEA) subsystems. Specifically, a stochastic semi-infinite fluid (SIF) is attached to the externally radiating face of the FE structural model as a radiation impedance to capture energy transfer propagating away from the fuselage structure.

At the high frequencies, where wavelengths are short compared to the dimensions of the structure and acoustic space, it is more efficient and desirable to represent the structural and acoustic modes statistically. The VA One SEA method[9] is used to obtain the space averaged vibro-acoustic response. The modal density, or the number of modes per unit frequency, and the modal overlap, the average number of modes within a typical half-power bandwidth, determine

the validity of the statistical assumptions in SEA and the accuracy of the computations, which, in turn, determines the lowest frequency band of the analysis.

CABIN SIMULATION MODELS

This section describes the simulation models created for the low frequency hybrid FE/SEA analysis and the high frequency SEA predictions.

Low Frequency Hybrid FE/SEA Models

Fuselage cabin simulation models for the low frequency vibro-acoustic analyses include structural FE models, Poro-Elastic Finite Element Method (PEM) subsystems, FE acoustic cavities, and a semi-infinite fluid (SIF). The PEM subsystems are included to represent the impedance of components designed to absorb or reflect sound energy when applied to FE surfaces, such as noise control treatments. It was assumed that pressurization affects primarily the radiation response of the fuselage skin panels between the frames and longitudinal stringers and was not modeled for the low frequency range where global modes of the structure dominate.

Structural Finite Element Models

The cabin structural models include the skin, longitudinal stringers, ring frames, floor, floor supporting beams, and bulkheads. For these predictions, the notional sidewall configuration was defined using geometry and material information of the Bombardier Dash-8 Q400 fuselage section described in Reference 5. The fuselage was modeled in MSC Patran[8] as a floor-equipped, stiffened cylinder. The fuselage is stiffened by thirty-nine evenly spaced ring frames and sixty-eight evenly spaced longitudinal stringers (longerons) framing a total of 2584 fuselage sidewall bays. The frame spacing is 0.58 m while the distance between stringers along the circumference is 0.124 m. The skin in each bay area between the ring frames and the longerons is represented by a matrix of two Quad4 elements in the circumferential direction and four Quad4 elements along the length of the cylinder. The floor is supported by thirty-nine horizontal floor beams with the same 0.58 m spacing as the ring frames and modeled with sixteen Quad4 elements along its width and four Quad4 elements between the beam supports. All beams are represented by Beam2 elements. An isometric view of the basic finite element model is shown in Figure 5.

The ring frames have a “U”-shaped cross-section while the longitudinal stringers have a “Z”-shaped cross-section.[5] The floor support beams also have a “U”-shaped cross section. The perimeter and area of the cross sections were computed, along with the cross-sectional property parameters such as the moments of inertia, the polar moment, torsional constant, distance from shear center to centroid and the shear stiffness factors. The resulting section properties for the ring frames, longitudinal stiffeners and the floor beams are listed in Table 2.

The skin of the fuselage consists of 1.6 mm-thick aluminum with a surface density of 4.35 kg/m^2. The mechanical material properties of the aluminum skin are shown in Table 3. The ring frames and the longitudinal stringers for the baseline configuration are also made of aluminum.

A honeycomb sandwich structure is used for the floor panels in the finite element model. Typically, product data sheets for honeycomb core materials[11] provide geometric and mechanical

properties such as cell size, density, compressive stabilized modulus and plate shear moduli in the ribbon direction and along the direction perpendicular to the ribbon. Although these are the most important mechanical properties, the remaining core elasticity moduli are needed as input properties for the finite element analysis. Nast[12] developed theoretical formulae to compute these core parameters. Experimental results in his research compared well with theoretical predictions. The formulae are valid for honeycomb cores with hexagonal type cells. A unit hexagonal cell can be defined by a rectangle containing three parts of the structure, one of which is double the foil thickness illustrated in Figure 6. The elasticity modulus of the core material E_f can be found by multiplying the transverse elasticity of the honeycomb E_3 with the ratio of the area of the unit cell A_{unit} and the actual cross section of the core material A_{actual}

$$E_f = \frac{A_{unit}}{A_{actual}} E_3 \tag{1}$$

The elasticity moduli E_1 and E_2 and the shear modulus G_{12} are shown to be dependent on the core material elasticity modulus E_f, the core Poisson's ratio ν_f, the foil thickness t, the cell size d, the cell wall length a, and the core angle φ.[12] These core cell dimensions are shown in Figure 6.

$$E_1 = \frac{t^3\left(1+\sin\varphi\right)E_f}{12a^3\cos^2\varphi\left(\frac{\cos\varphi}{3}-\frac{1+\cos\varphi}{8}\right)\left(1-\nu_f^2\right)} \tag{2}$$

$$E_2 = \frac{t^3\cos\varphi E_f}{a^3\sin^2\varphi\left(1+\sin\varphi\right)\left(1-\nu_f^2\right)} \tag{3}$$

$$G_{12} = \frac{t^3\left(1+\sin\varphi\right)E_f}{a^3\cos\varphi\left(6.25-6\sin\varphi\right)\left(1-\nu_f^2\right)} \tag{4}$$

The dimensions of the honeycomb cells for the floor panels are listed in Table 4 and were used, in combination with the available manufacturer material data, to compute the three-dimensional orthotropic mechanical material properties for the floor aramid honeycomb core listed in Table 5. Unidirectional, 0.71 mm thick S-2 glass reinforced epoxy facings were selected as face sheets and bonded to the aramid honeycomb core in a construction similar to other typical aircraft flooring panels.[13] The two-dimensional orthotropic material properties of the S-2 glass face sheets are listed in Table 6. The mechanical material properties of the face sheets and the 8.92 mm thick honeycomb core, along with thickness and orientation values, were entered as laminated composites in the MSC Patran modeler. The total thickness of the stacking sequence is 10.34 mm with a total density of 377 kg/m^3.

Poro-Elastic Finite Element Method (PEM) Models

PEM models were developed for the fuselage trim, the floor coverings, the seats, and the overhead bins to more accurately represent their poro-elastic properties. The PEM solver in VA One is based on a finite element implementation of the poro-elastic, elastic and acoustic equations of motion and is used to generate the modal impedance matrix coupled to the structural and acoustic FE subsystems. A PEM subsystem may encompass foam material, fiber material,

elastic solid structures, limp structures or acoustic fluids. Adjacent PEM subsystems must share the same nodes at their interface.

The interior trim and the floor poro-elastic layer were modeled using solid Hex8 elements in the MSC Patran finite model of the LCTR2 fuselage. A maximum length of 0.145 m was conveniently selected for the element size as it equates to four elements between ring frames (bay length is 0.58 m). The volumes above and below the floor were subsequently meshed with Hex8 elements as well. Instead of accurately modeling the seats and overhead bins they were, in an initial approach, "carved out" of the FE volume above the floor. The resulting FE models of the seats and overhead bins were saved in binary files, imported in VA One and converted to PEM subsystems. An isometric view of the rudimentary PEM models for the seats and the overhead bins is presented in Figure 7. A cross-sectional view is shown in Figure 8.

The trim arrangement consisted of a thin airgap, a porous absorption material and a trim panel. The honeycomb polymer trim panels, typical for a Q400 aircraft,[14] were installed at a distance of 81 mm from the fuselage skin. The trim panels were 3 mm thick with a surface density of 0.765 kg/m^2 and an estimated loss factor of 0.02. The mechanical material properties of the trim panels are listed in Table 7. The trim absorption material consisted of 80 mm thick melamine foam layer with a loss factor of 0.17. The Biot properties of the melamine foam are tabulated in Table 8, while the diffuse field absorption coefficients are shown in Figure 9. The thin airgap layer (1 mm) was included to account for the trim absorption material not being bonded to the fuselage skin. The thin airgap and the melamine foam were modeled with solid elements, while shell elements were used for the trim panel. An isometric view of the interior trim PEM model is shown in Figure 7 and a cross-sectional view in Figure 8.

The Biot properties of foam typically used in seats are listed in Table 8. The diffuse field absorption coefficients of a 25.4 mm thick sample of the foam as a function of one-third octave band center frequency are included in the VA One materials data base and are shown in Figure 9 for rigid wall boundary conditions.

The floor covering consisted of a 48.8 mm thick, fiber poro-elastic material and a 3 mm thick floor surface with an estimated loss factor of 0.1. The mechanical properties of the floor surface panels are listed in Table 7, while the Biot properties of the poro-elastic layer (felt) are tabulated in Table 8. The PEM model of the floor covering is presented in Figure 7 and Figure 8.

The overhead bins were assumed to be stowed and were modeled with equivalent isotropic solid material properties (Table 7). Figure 7 and Figure 8 show the overhead bins PEM models.

To allow an accurate analysis the mesh density of the PEM model has to comply with the requirement of at least four linear elements per wavelength. The shortest wavelengths of the propagating waves in the material as a function of one-third octave band center frequency were computed in VA One and are shown in Figure 10. The propagating wavelengths in the seat foam are the shortest. At 100 Hz the wavelength is about 0.30 m. The maximum element size of 0.145 m used in the finite element models accommodates only two elements for the shortest wavelength at 100 Hz. However, VA One provides an option to use quadratic elements for the PEM analysis, whereby mid-side nodes are automatically added to the mesh, essentially doubling the number of elements per wavelength. Exercising this option resulted in at least four elements per wavelength allowing accurate PEM analyses up to and including the 100 Hz one third octave band for the seat foam, and up to 200 Hz for the melamine foam and the floor poro-elastic layer.

Acoustic Finite Element Models

The acoustic upper cavity in Figure 8 was created in MSC Patran by subtracting the "carved out" finite elements models of the seats, overhead bins, floor arrangement and trim arrangement from the total volume above the floor bounded by the fuselage skin and the end bulkheads. The acoustic upper cavity was assigned properties of air for the pressurized aircraft cabin (Table 9) and divided in two parts, the space forward of the tiltrotor plane and the acoustic volume aft of the tiltrotor plane. The forward and aft acoustic upper cavity models were saved in binary files and imported in VA One as acoustic FE subsystems. Figure 11 shows the forward and aft acoustic upper cavities relative to the tiltrotor plane. The Hex8 elements in the meshed volume below the floor were also assigned properties of air for the pressurized aircraft to constitute the acoustic lower cavity (Figure 8).

High Frequency SEA Models

Predictions in the low frequency region were based on the structural and acoustic modes of the different subsystems and the deterministic description needs detailed information of the local geometry, material properties and boundary conditions. At the higher frequencies the modal density and modal overlap increase significantly and the modes in the subsystems are described statistically. Less detail is required and only the average response of the subsystem is predicted. The porous noise control treatments are weakly coupled to the structure and mainly provide sound absorption.

Structural SEA Model

The fuselage is supported by thirty-nine evenly spaced ring frames bounding thirty-eight axial segments. Nineteen SEA subsystems of the floor, and nineteen subsystems of the curved fuselage sections above and below the floor, each two segments long, were created for a total of fifty-seven subsystems (the subsystems are shown in Figure 12 and were shrunk for clarity). This allows computation of the energy flow and structural response at nineteen subsystems along the fuselage of the cabin. The fuselage skin, the longitudinal stringers and the ring frames were represented by ribbed plate subsystems with as input the skin material and mechanical properties, the beam material properties, the moments of inertia, the torsional constants, the cross-sectional areas, the locations of the shear center relative to the neutral axis of the section, the centroid offsets and the beam spacing. The floor and the supporting floor beams were modeled in a similar manner. Pressurization, the difference between internal and external pressures, was used in VA One to define the in-plane tensions and resulting geometric stiffness of the bay skin panels between the ring frames and the longitudinal stringers.

Acoustic SEA Model

For the high frequency analysis the fuselage was divided into nineteen identically-sized sections above the floor and nineteen sections below the floor. The thirty-eight acoustic cavity sections are shown in relation to the tiltrotor plane in Figure 13. The frequency dependent effective absorption in the cabin was taken as the upper bound of the average of experimental acoustic absorption data available for high-speed propeller driven aircraft[15,16] and includes the combined influence of the floor covering, the trim and the seats. The experimental average cabin absorption coefficient is plotted in Figure 14 as function of one-third octave band center frequency.

EXCITATION MECHANISMS

Turbulent Boundary Layer Excitation

LCTR2 broadband noise due to an attached turbulent boundary layer were predicted for cruise flight conditions at a vehicle speed of 556 km/hr, an altitude of 8534 m, rotational Mach number of 0.35 and a helical tip Mach number of 0.61. The design parameters are listed in Table 1.

The turbulent boundary layer noise was modeled as a fluctuating pressure spectrum in the acoustic prediction code VA One.[9] A different boundary layer excitation was applied at each of the nineteen fuselage sidewall sections to account for the increase in boundary layer thickness as a function of the distance from the nose of the vehicle. The turbulent boundary layer thickness δ at distance x_0 from the nose of the tiltrotor vehicle was computed from the relation

$$\delta = 0.37 \frac{x_0}{Re^{0.2}} \tag{5}$$

where Re is the Reynolds number, which is defined by

$$Re = \frac{U_0 x_0}{\upsilon} \tag{6}$$

The free stream velocity U_0, the kinematic viscosity υ and the properties of air at cruise altitude are listed in Table 9. The computed turbulent boundary layer thickness as function of distance from the LCTR2 nose is listed in Table 10. Both Cockburn/Robertson and Efimtsov turbulent boundary layer semi-empirical models are available in VA One, each having different, frequency dependent power spectral density levels. To achieve better parameter control, the Cockburn/Robertson and Efimtsov turbulent boundary layer models were computed outside the program after which the excitation power spectral densities were imported into VA One.

Cockburn and Robertson

The power spectral density of the attached turbulent boundary layer was obtained by Cockburn/Robertson using vibration response measurements of spacecraft shrouds to in-flight fluctuating pressures.[17] The power spectral density Φ_C, non-dimensionalized by the free stream velocity U_0, the local boundary layer thickness δ and the dynamic pressure q_∞ is defined by

$$\frac{\Phi_C(f) U_0}{q_\infty^2 \delta} = \frac{(0.006)^2}{\left(\frac{f_0 \delta}{U_0}\right)\left[1+\left(\frac{f}{f_0}\right)^{0.9}\right]^{2.0}\left(1+0.14M^2\right)} \tag{7}$$

where $q_\infty = \frac{1}{2}\rho U_0^2$; $M = \frac{U_0}{c_0}$ .and $f_0 = 0.346\frac{U_0}{\delta}$.

The narrowband spatial correlation function R_C between two points ε and η along the flow direction z is given by[9,17]

$$R_C\left(\varepsilon,\eta,\omega\right)=\exp\left[-\frac{c_z\left|\Delta z\right|}{d}-\frac{c_w\left|\Delta w\right|}{d}\right]\exp\left[-ik_c\Delta z\right] \tag{8}$$

where c_z and c_w are the spatial correlation decay coefficients in the flow and cross-flow directions, $k_c=\omega/U_c$ is the convection wavenumber, and d is defined by

$$d=\left[k_c\sqrt{1+\left(\frac{8}{3k_c\delta}\right)^2}\right]^{-1} \tag{9}$$

The convection speed U_c was chosen to be 0.7 times the free stream velocity U_0, and c_z= 0.1 and c_w=0.72.

Efimtsov

The power spectral density Φ_E of the turbulent boundary layer pressure fluctuations according to the empirical model by Efimtsov is given by[18,19]

$$\Phi_E\left(\omega\right)=2\pi U_\tau^3\rho^2\delta\frac{\alpha\beta}{\left(1+8a^3S_t^2\right)^{1/3}+\alpha\beta Re_\tau\left(S_tRe_\tau\right)^{10/3}} \tag{10}$$

where $U_\tau=U_0(c_f/2)^{0.5}=(\tau/\rho)^{0.5}$ is the friction velocity, $S_t=\omega\delta/U_\tau$ is the Strouhal number, $\alpha=0.01$, $\beta=[1+(3000/Re_\tau)^3]^{1/3}$ and $Re_\tau=U_\tau\delta/\upsilon$ is the Reynolds number. The root-mean-square pressure equals $(\Phi_E(f)\Delta f)^{-0.5}$ in which Δf is the bandwidth.

The spatial correlation function R_F for a free stream velocity at M<0.75 with convection velocity U_c is given by

$$R_F\left(\varepsilon,\eta,\omega\right)=\exp\left\{-\frac{\left|\varepsilon\right|}{\delta}\left[\left(\frac{a_1S_t}{U_c/U_l}\right)^2+\frac{a_2^2}{S_t^2+\left(a_2/a_3\right)^2}\right]^{0.5}-\frac{\left|\eta\right|}{\delta}\left[\left(\frac{a_4S_t}{U_c/U_l}\right)^2+\frac{a_5^2}{S_t^2+\left(a_5/a_6\right)^2}\right]^{0.5}\frac{i\varepsilon\omega}{U_c}\right\} \tag{11}$$

where the ratio of velocities is defined by

$$\frac{U_c}{U_l}=a_8S_t^{0.2}\left[\frac{1+\left(a_9S_t\right)^2}{1+\left(a_{10}S_t\right)^4}\right]^{0.1} \tag{12}$$

and the coefficients a_1 through a_6 and a_8 through a_{10} are empirical constants which are listed in Table 11. The constant a_7 is not used for Mach numbers lower than 0.75.

The convection wavenumber $k(f)$ in the direction of the flow is ω/U_c and equals zero in the direction perpendicular to the flow. For Mach numbers lower than 0.75 the Efimtsov boundary layer decay coefficients c_x and c_y are given by[18,19]

$$c_{x,y}(f) = \frac{1}{\delta}\left[\left(\frac{a_{1,4}S_t}{U_c/U_l}\right)^2 + \frac{a_{2,5}^2}{S_t^2 + \left(a_{2,5}/a_{3,6}\right)^2}\right]^{0.5}\left(\frac{\omega^2}{U_c^2} + \frac{7.11}{\left(0.37X_0R_e^{-0.2}\right)^2}\right)^{-0.5} \quad (13)$$

Turbulent Boundary Layer Excitation Comparison with Measured Data

The Cockburn/Robertson and Efimtsov predicted pressure power spectral densities are compared with measurements by Bhat[20] on a Boeing 737 aircraft in Figure 15. The flight test conditions for the Boeing 737 turbulent boundary layer measurements are summarized in Table 12. The measurements at Mach number 0.78 at a distance of 8.81 m from the nose of the aircraft were believed by the author to represent the turbulent boundary layer noise, masking any noise associated with the engine inlet. In the report[20] a smooth line was drawn through the raw data resulting in the dashed spectral density curve in Figure 15. The pressure power spectral density was constant up to about 500 Hz. The Efimtsov predictions for those frequencies are constant as well although they overpredict the measured data by a factor of 1.62 or about 2 dB. Above 500 Hz the measured spectral density levels decrease rapidly with increasing frequency and is better represented by the Cockburn/Robertson predicted values. However, the decay rate in the Boeing 737 measurement curve was believed to be steeper than expected for a smooth (fuselage) surface and level flight,[20] due to a higher than expected wall roughness and a 5 degree body angle of attack. Assuming the decay rate of the measured data is less steep then a good estimate above 500 Hz will be a curve bounded by the Efimtsov and the Cockburn/Robertson predictions. Therefore, in subsequent analyses with turbulent boundary layer excitation over the full length of the fuselage cabin the results from the Efimtsov model will be used over the entire frequency range of interest (6-8000 Hz), while the Cockburn/Robinson results will be considered in the high frequencies when lower than Efimtsov.

ANALYSES

The hybrid FE approach in VA One[9] was used to compute the low frequency acoustic response in the cabin due to the Efimtsov turbulent boundary layer excitation over the frequency range 6–141 Hz with a 1 Hz bandwidth (141 Hz is the limiting frequency in the 125 Hz one-third octave band and is needed for conversion from narrowband to one-third octave band). Subsequently, the SEA approach was used to predict the interior noise for the 125–8000 Hz one-third octave bands due to either the Cockburn/Robertson or the Efimtsov turbulent boundary layer excitation. The two analysis methods overlap in the 125 Hz band.

Low Frequency Hybrid FE/SEA Analysis

Structural Modal Response

The in-vacuo structural modal response of the fuselage model, including the fuselage skin, ring frames, longitudinal stringers, the floor and the floor supports, was computed using MSC Nastran 2010.[10] Simply supported boundary conditions were assumed at the aft bulkhead location and the forward flight deck entrance. Future analyses will include more realistic boundary conditions to reflect the fuselage being supported by the wings at the wing box interface. The structural modal analysis results were then imported into VA One. A default 1%

structural damping loss factor was assumed. The lowest structural mode of the fuselage occurred at 9.07 Hz. The mode is a first order axial mode as it has no nodal lines between the aft bulkhead and the front flight deck access. Figure 16 shows an isometric view of the first mode while a cross-sectional view of the circumferential modal pattern is displayed in Figure 17. The number of structural modes in the one-third octave bands with center frequencies 5–160 Hz is listed in Table 13.

Acoustic Modal Response

The acoustic modes in the cavities above and below the floor were computed by a modal analysis in VA One. The lowest acoustic mode, in the axial direction, was predicted to occur at 5.7 Hz (Figure 18) and is a first-order axial mode having one nodal line with the highest interior sound pressure levels occurring at the bulkhead and the forward flight deck wall. The first cross-sectional acoustic mode, which may efficiently couple to structural circumferential mode(s), occurred at 73.8 Hz and is shown in Figure 19. The number of acoustic modes computed in each one-third octave band is listed in Table 13.

Poro-Elastic Modal Impedance Matrix

The modal impedance matrix of the contiguous PEM groups of seats, overhead bins, floor arrangement and trim configuration subsystems, which are coupled to the modes of the FE fuselage system and the modes of the FE acoustic cavity systems, is computed as an intermediate result.

Cabin Interior Noise Predictions

VA One computes the cabin sound pressure levels in the low frequency region by coupling the in-vacuo structural modes, the rigid-boundary acoustic modal parameters and the PEM modal impedance matrix; applying the turbulent boundary layer excitation; and accounting for energy propagating away from the structure by including a radiation impedance. The sound pressure level predictions for the Efimtsov turbulent boundary layer excitation were performed for the LCTR2 cabin forward and aft of the tiltrotor plane in the 6–141 Hz frequency bands using a 1 Hz analysis bandwidth. The predicted mean narrowband interior sound pressure levels are shown in Figure 20 along with the averaged sound pressure levels for the entire cabin.

At low frequencies the interior cabin sound pressure level variations are determined by the coupled acoustic and structural modal responses. The number of structural and acoustic modes in each of the one-third octave bands with center frequencies 5-160 Hz is listed in Table 13. The modal frequencies of the structural and acoustic modes below 20 Hz are tabulated in Table 14. The first, second, and third axial acoustic modes occur at 5.75 Hz, 11.6 Hz and 17.6 Hz respectively, and these are the only three acoustic cabin modes below 20 Hz. The acoustic mode number indicates the number of nodal lines in the response. Eleven structural modes were identified below 20 Hz and their axial mode numbers are included in Table 14 as well. The structural mode number indicates the number of anti-nodes (maximum response between nodal lines), or the number of nodal lines plus one.

The second order axial acoustic mode at 11.6 Hz (Figure 21) has two nodal lines and a maximum response in the center. The closest structural modes are first-order axial resonances at 11.3 Hz (Figure 22) and 11.5 Hz (Figure 23). The acoustic mode and the two structural modes all

have a maximum response in the center and similar spatial characteristics. Since their modal resonance frequencies are also very close to one another the acoustic and structural modes will couple and exchange energy resulting in a maximum predicted sound pressure level at 12 Hz in Figure 20. The resulting variation of the predicted sound pressure levels in the cabin interior at 12 Hz is shown in Figure 24, with the local maxima and minima at the locations of the maximum and zero acoustic modal responses, respectively. Peak interior sound pressure levels coincide with the maximum acoustic modal response in the center and near both ends of the cabin. Sound pressure level variations inside the cabin are as high as 18 dB.

The third-order axial acoustic resonance at 17.6 Hz (Figure 25) couples well with the second-order structural modes at 17.3 Hz (Figure 26) and 18.7 Hz (Figure 27) due to the spatial characteristics of the acoustic modal pressures and the structural modal displacements. Both the acoustic and the structural modes have a nodal line in the center and maximum responses on either side. The resulting distribution of the predicted sound pressure levels in the cabin at 17 Hz is shown in Figure 28 and is similar to the variations in the acoustic modal response. Peak interior sound pressure levels coincide with the maximum acoustic modal response at approximately one-third and two-third of the length of the cabin. Sound pressure level variations inside the cabin are as high as 16 dB. The predicted space averaged interior sound pressure levels show a peak at 17 Hz as shown in Figure 20. All the peaks up to 70 Hz in the sound pressure level predictions of Figure 20 are attributed to the coupling of axial acoustic modes with axial structural modes. As frequency increases, progressively higher-order axial modes join the overall modal response. The first cross-sectional acoustic mode was computed at 73.8 Hz (Figure 19) and is characterized by a vertical nodal line in the tiltrotor plane cross-section. Figure 29 shows another resonance response with a vertical nodal line at 89.2 Hz in the tiltrotor plane cross-section of the aft acoustic cavity. The 89.2 Hz frequency is in the 100 Hz one-third octave band which contains 93 structural and 25 acoustic resonant modes (Table 13). Several non-resonant modes participate in the modal response of the 100 Hz one-third octave band as well. Figure 30 shows a cross-sectional mode with a horizontal nodal line at 128.9 Hz in the 125 Hz one-third octave band. The number of acoustic and structural resonances in the 125 Hz band equals 21 and 129 respectively (Table 13), and the number of modes participating has grown so large that the individual cross-sectional modes such as in Figure 29 and Figure 30 only partially contribute to the global cabin noise. However, they still may cause local hotspots of sound, especially close to the fuselage sidewall where they may efficiently couple to circumferential structural modes.

High Frequency SEA Analysis

A high frequency SEA analysis was performed for the structural and acoustic subsystems, while being exposed to either the Cockburn/Robertson or the Efimtsov turbulent boundary layer excitation. The modal density in the acoustic space above the floor was estimated in VA One for the one-third octave frequency bands of 100–8000 Hz as shown in Figure 31. The modal density exceeds approximately one mode per Hz in the 125 Hz and higher bands, sufficient to justify the high frequency SEA analysis. A semi infinite fluid (SIF) representing an unbounded exterior acoustic space was connected to the nineteen curved structural subsystems of the upper as well as the lower fuselage sections to serve as an acoustic radiation impedance. The curved shell of the fuselage was exposed to a pressure differential between the external atmospheric pressure at the cruise altitude of 8534 m and the pressure of the effective equivalent cabin altitude of 2438 m (Table 9). The pressurization of 42.3 kPa was used in VA One to define the in-plane tensions and resulting geometric stiffness of the fuselage skin panels.

Cabin interior sound pressure levels due to the Cockburn/Robertson turbulent boundary layer excitation were predicted for the nineteen acoustic subsystems in the cabin above the floor for the 125 Hz and higher one-third octave frequency bands. The subsystem sound pressure levels along with their averaged values are plotted in Figure 32. The highest interior sound pressure levels are in the aft cabin subsystem at the farthest distance from the nose of the vehicle where the turbulent boundary layer thickness has its highest value.

The sound pressure level predictions due to the Efimtsov turbulent boundary layer excitation for the nineteen cabin subsystems are shown in Figure 33 along with their space averaged levels for the entire cabin. Highest sound pressure levels are again in the back of the cabin. The spread between the subsystem levels is greater than for the Cockburn/Robertson model due to the greater spread in their excitation spectral densities.

LCTR2 Analysis Results for the Consolidated Frequency Range

The hybrid FE predicted cabin averages of the LCTR2 sound pressure levels forward and aft of the tiltrotor plane due to Efimtsov boundary layer excitation were presented in Figure 20 as narrowband data with a resolution of 1 Hz. To assess the levels in the human audible frequency range (above 20 Hz) the narrowband predictions were converted to one-third octave bands and data in the 20-125 Hz bands are plotted in Figure 34. The SEA predicted cabin averaged sound pressure levels due to the Efimtsov and the Cockburn/Robinson excitations are shown in the same Figure 34. The predictions for the hybrid FE and SEA methods for the Efimtsov model differ by less than 1 dB in the 125 Hz one-third octave band. However, this good agreement may be fortuitous as the interior sound pressure levels are averaged over the cabin, and several parameters like loss factors, acoustic absorption values, boundary conditions, trim treatment and others are modeled differently in the low and high frequency approaches. Also, pressurization was not modeled for the hybrid FE approach but was included in the SEA analysis.

Contour plots for the two prediction methods in the 125 Hz band are plotted in Figure 35 for the SEA method and in Figure 36 for the hybrid FE method. The SEA predictions show the nineteen acoustic subsystems, each of which having a constant subsystem sound pressure level. The hybrid FE predictions in Figure 36 show that the interior sound pressure level distribution is governed by the axial and cross-sectional modal behavior in the cabin interior. From an overall perspective the sound pressure level distribution for both the SEA and hybrid FE predictions show comparable characteristics. The cabin sound pressure level variation is as high as 18 dB for the SEA predictions and 20 dB for the hybrid FE results.

The space averaged cabin interior sound pressure levels predicted for the high frequency Cockburn/Robertson model are also plotted in Figure 34 as it was assumed previously that the prediction curve most likely would be in between the two high frequency analyses. The different representations of the turbulent boundary layer spectra for the Cockburn/Robertson and Efimtsov models lead to large differences in the high frequency cabin interior noise predictions (13 dB at 2000 Hz in Figure 34). However, this may be of little concern for human response issues as both models predict relatively low interior noise levels with the higher Efimtsov excitation dropping below 50 dB for the 2000 Hz and higher frequencies.

Bombardier Q400 Predictions Compared with Measurements

Although no tightly controlled experimental acoustic data are available to validate the LCTR2 predictions a comparison is made with a 2002 study conducted by the National Institute for Occupational Safety and Health (NIOSH)[18] to evaluate noise exposure by flight attendants on selected Bombardier aircraft among which the Dash-8 Q400 turboprop. In this survey spectral noise measurements were made with a Larson-Davis Laboratory Model 2800 real-time analyzer and a Larson-Davis Laboratory Model 2559 half-inch diameter random incidence microphone. The microphone had a frequency response range (± 2 dB) from 4 to 21000 Hz and was connected to the analyzer with a 1.8 m cable. One-third octave bands consisting of center frequencies from 25 Hz to 20 kHz were integrated for 15 seconds and stored in the analyzer. Samples were acquired at cruise altitude during level flight. The Bombardier Q400 aircraft is equipped with a noise and vibration suppression (NVS) system that actively suppresses propeller tones before reaching the occupants in the cabin. The NVS system was operational during the noise measurements.

The Bombardier Q400 one-third octave band spectrum measured during cruise conditions in the front of the cabin is plotted in Figure 37 showing peak levels at the propeller blade passage frequency in the 80 Hz one-third octave band and harmonics in the 160 and 315 Hz bands. Superimposed on this plot are the predicted interior noise levels due to Efimtsov and Cockburn/Robertson turbulent boundary layer excitation averaged over the cabin space. The cruise conditions for the Q400, used in the predictions, are summarized in Table 15. The low frequency (< 125 Hz) Efimtsov model overpredicts the broadband components of the Q400 spectrum by up to 9 dB at 25 Hz. However, inaccuracies in the low-frequency predictions are associated with assumptions made for material properties, structural and acoustic modal parameters and boundary conditions, structural damping and acoustic absorption. Also, the in-flight measurements have several unknowns including detailed test conditions, the precise measurement location and the proximity of that location to the sidewall trim and seat surfaces. Finally, applying A-weighting to the predicted data (from -50.5 at 20 Hz to -16.1 at 125 Hz) to account for the fact that the human ear is not as sensitive to the lower frequencies reduces the levels in the 20-125 Hz bands to less than 53 dB, which are considered acceptable cabin noise levels. The cabin averaged high frequency predictions with both the Efimtsov and Cockburn/Robinson models show (much) lower levels than the one-third octave band sound pressure levels measured for the Q400. In addition to the argument of assumptions in the predictions and unknowns in the measurements, it has to be noted that other sources than the turbulent boundary layer excitation may have contributed to the measured noise at the high frequencies such as the pressurization and air conditioning systems, passengers, equipment, lavatories, etc. Since the highest noise levels due to turbulent boundary layer excitation occur in the aft cabin the Efimtsov predictions for that location are also plotted in Figure 37 for comparison with the measured levels in the front of the Q400 cabin. The averaged cabin noise levels in the LCTR2 during cruise conditions (Figure 34) are predicted to be lower than those for the Q400 aircraft in cruise (Figure 37), due to lower cruise speed (Mach 0.51 versus Mach 0.60 for the Q400) and higher cruise altitude (8534 m versus 7620 m for the Q400). The cruise noise levels predicted for the LCTR2 cabin are thus comparable or lower than measured in the Q400 cabin and thus will be acceptable to passengers and crew. It should be emphasized that only turbulent boundary layer noise is considered here and contributions due to thickness and loading noise from the tiltrotor blades and mechanical noise radiated by the mid-wing gearbox will be the subject of another study.

SUMMARY

A prediction scheme was established to compute sound pressure levels in the cabin of the notional Large Civil Tiltrotor (LCTR2) due to turbulent boundary layer flow over the fuselage during cruise flight conditions. Structural and acoustic finite element models were created in MSC Patran and a modal analysis of the fuselage structure was performed in MSC Nastran. An acoustic modal analysis of the cabin space was completed in VA One. The finite element geometry along with the structural modal parameters and mode shape deflection information were subsequently imported into VA One to model the fuselage, the cabin acoustic space and the cabin interior components as energy transmitting, storing and receiving vibro-acoustic mechanisms. Poro-Elastic Finite Element Method (PEM) models were developed for the seats, the overhead bins, the fuselage trim, and the floor coverings to more accurately represent their poro-elastic and structural properties. Cockburn/Robertson and Efimtsov turbulent boundary layer excitation models were applied to nineteen segments of the fuselage to represent the variation of the excitation spectra with distance from the nose of the vehicle. Cabin interior sound pressure levels were predicted employing a narrowband (1 Hz) hybrid Finite Element (FE) analysis for the low frequencies (6-141 Hz) and a Statistical Energy Analysis (SEA) method for the high frequency one-third octave bands (125-8000 Hz). It is shown that the interior sound pressure level distribution in the low frequencies is governed by interactions between individual structural and acoustic modes. Only axial acoustic modes were computed below 73.8 Hz at which frequency the first cross-sectional mode was predicted. Peak sound pressure levels occurred at the same locations as the maxima in the acoustic modal response. Interior sound pressure level predictions for the low and high frequencies were combined and averaged over the entire cabin volume. The spatially averaged predicted interior sound pressure levels for the low frequency hybrid FE and the high frequency SEA analyses, due to the Efimtsov turbulent boundary layer excitation, were within 1 dB in the common 125 Hz one-third octave band. However, this good agreement may be fortuitous due to the assumptions in the modeling parameters and the averaging of the cabin sound pressure levels. The averaged interior noise levels for the notional LCTR2 cabin due to turbulent boundary layer excitation were predicted lower than the levels in a Bombardier Q400 aircraft cabin during cruise flight due to the higher altitude and lower cruise Mach number of the LCTR2 and will be acceptable to crew and passengers.

ACKNOWLEDGEMENTS

This work was performed under the Analytical Mechanics Associates, Inc. Contract Number NNL12AA09C. Dr. Randolph H. Cabell, Technical Direction Notice (TDN) owner.

REFERENCES

1. Johnson, W., Yamauchi, G.K., and Watts, M.E.: NASA Heavy Lift Rotorcraft Systems Investigation. NASA TP-2005-213467, September 2005.
2. Acree, C.W., Yeo, H., and Sinsay, J.D.: Performance Optimization of the NASA Large Civil Tiltrotor. International Powered Lift Conference, London, UK, July 2008; also NASA TM-2008-215359, June 2008.
3. Acree, C.W. Jr.: Integration of Rotor Aerodynamic Optimization with the Conceptual Design of a Large Civil Tiltrotor, NASA Ames, ARC-E-DAA-TN1176, January 2010.

4. Grosveld, Ferdinand W. and Cabell, Randolph, H.: Preliminary assessment of the interior noise environment in the Large Civil Tiltrotor (LCTR2). nc11_129, Proceedings of Noise-Con 2011, Portland, Oregon, USA, 25-27 July 2011.
5. Gardonio, P. and Gonzalez Diaz, C.: Bombardier Dash-8 Q400 Fuselage Section with Five Decentralized Velocity Feedback Control Units. ISVR Technical Memorandum 983. Institute of Sound and Vibration Research, Southampton, UK, January 2009.
6. Tubbs, Randy L.: NIOSH Health Hazard Evaluation Report HETA 2002-0354-2931. Horizon Air. Seattle, Washington. February 2004.
7. Aviation International News: Bombardier considers stretch variant for Q400. Paris Air Show. Air Transport and Cargo Aircraft. June 2009.
8. MSC Patran 2012. MSC Software Corporation, Santa Ana, California, 2012.
9. VA One 2011 User's Guide. ESI Group North America, December 2011.
10. MSC Nastran 2010.1.1. MSC Software Corporation, Santa Ana, California, 2012.
11. HexWeb HRH-10 Aramid Fiber/Phenolic Honeycomb Product Data Sheet. Hexcel Corporation, Dublin, CA, 2012. (http://www.hexcel.com)
12. Nast, E.: On Honeycomb-Type Core Moduli. AIAA -97-1178, Proceedings of the 28th AIAA/ASME/ASCE/AHS/ASC SDM Conference, 1997.
13. Gillfloor 4017T Light Weight Aircraft Flooring Panel. M.C. Gill Corporation, El Monte, CA, March 2001.
14. Alujević, Neven: Smart double panel with decentralised active damping units for the control of sound transmission. Institute of Sound and Vibration Research, University of Southampton, England, August 2008. (http://eprints.soton.ac.uk)
15. Wilby, J.F., Rennison, D.C. and Wilby, E.G.: Noise Control Predictions for High-Speed, Propeller-Driven Aircraft. AIAA-80-0999, June 1980.
16. Rennison, D.C., Wilby, J.F., Marsh, A.H., and Wilby, E.G.: Interior Noise Control Prediction Study for High-Speed, Propeller-Driven Aircraft. NASA Contractor Report 159200, NASA Langley Research Center, Hampton, Virginia, September 1979.
17. Cockburn, J.A., Robertson J.E.: Vibration Response of Spacecraft Shrouds to In-flight Fluctuating Pressures. *Journal of Sound and Vibration*, 1974, 33(4), 399-425.
18. Efimtsov, B.M.: Characteristics of the field of turbulent wall pressure fluctuations at large Reynolds numbers. *Soviet Physics Acoustics*, 1982, 28, pp. 289-292.
19. Miller, T.S., Gallman, J.M., and Moeller, M.J.: Review of Turbulent Boundary-Layer Models for Acoustic Analysis. *AIAA Journal of Aircraft*, Vol. 49, No. 6, November-December 2012, pp. 1739-1754.DOI: 10.2514/1.C031405
20. Bhat, V.W.: Flight test measurement of measurement of exterior turbulent boundary layer pressure fluctuations on Boeing Model 737 airplane. *Journal of Sound and Vibration* 1971, 14(4), pp. 439-457.
21. Grosveld, Ferdinand W., Cabell, Randolph H., and Boyd Jr., Doug D.: Interior Noise Predictions in the Preliminary Design of the Large Civil Tiltrotor (LCTR2). Proceedings of the AHS International 69th Annual Forum and Technology Display, 21-23 May 2013.

TABLES

Table 1. Design parameters for the LCTR2.

Parameter		LCTR2
Passengers		90
Range	[km]	1800
Maximum cruise speed	[km/hr]	555.6
Maximum operating altitude	[m]	8534
Fuselage diameter	[m]	2.74
Maximum cabin width	[m]	2.56
Cabin length	[m]	21.84
Number blades	[-]	4
Tip speed cruise	[m/s]	107
Rotational Mach number	[-]	0.35
Helical tip Mach number	[-]	0.61
BPF cruise	[Hz]	6.75
RPM cruise	[rpm]	101
Rotor radius	[m]	9.906
Engine power	[kW]	10067
Clearing rotor tip-fuselage	[m]	0.457

Table 2. Section properties of the longitudinal stringers, ring frames and floor support beams.

Property Parameter Shape	Label		Ring Frames 'U'	Longitudinal Stringers 'Z'	Floor Beams 'U'
Cross sectional area	A	[m^2]	0.0002925	0.0001025	0.0002607
Perimeter	P	[m]	0.2390	0.0870	0.2238
Moments of inertia	Ixx	[m^4]	2.299E-7	7.286E-9	1.532E-7
	Iyy	[m^4]	1.249E-8	1.848E-9	1.516E-8
	Ixy	[m^4]	0.0	-2.652E-9	0.0
Polar Moment	J	[m^4]	2.424E-7	9.134E-9	1.684E-7
Torsional constant	Q	[m^4]	6.094E-10	2.070E-10	4.922E-10
Distance shear center	$d_{horizontal}$	[m]	0.0	0.0	-0.01386
to centroid	$d_{vertical}$	[m]	-0.01099	0.0	0.0
Shear stiffness factors	K1		0.60684	0.43902	0.53624
	K2		0.35043	0.43902	0.42030

Table 3. Mechanical material properties of the skin, ring frames and longitudinal stringers.

	Density ρ [kg/m^3]	Young's modulus E_{11} [GPa]	Shear modulus G_{12} [GPa]	Poisson's ratio ν_{12} [-]
Aluminum	2720	71.0	26.7	0.33

Table 4. Dimensions of the cells in the honeycomb core of the floor panels. The geometric parameters a, b, t, d and φ are defined in Figure 6.

	a [mm]	**b** [mm]	**t** [mm]	**d** [mm]	**φ** [deg]
Floor	1.83	1.83	0.076	3.175	30

Table 5. Three-dimensional orthotropic material properties of the floor honeycomb core.

	Density	**Thickness**	**Young's moduli**			**Shear moduli**		
	ρ [kg/m^3]	**t** [mm]	**E_{11}** [MPa]	**E_{22}** [MPa]	**E_{33}** [MPa]	**G_{12}** [MPa]	**G_{31}** [MPa]	**G_{23}** [MPa]
Aramid honeycomb floor	144	8.92	2.30	1.77	621	0.407	120.7	75.9

Table 6. Two-dimensional orthotropic material properties of the floor fiberglass face sheets.

	Density	**Thickness**	**Young's moduli**		**Shear modulus**	**Poisson's ratio**
	ρ [kg/m^3]	**t** [mm]	**E_{11}** [GPa]	**E_{22}** [GPa]	**G_{12}** [GPa]	**ν_{12}** [-]
S2-glass unidirectional face sheet	1840	0.712	56	18	7.5	0.27

Table 7. Mechanical material properties of the floor surface panels, the trim panels and the overhead bins.

	Density	**Surface mass**	**Thickness**	**Young's modulus**	**Shear modulus**	**Poisson's ratio**
	ρ [kg/m^3]	**m** [kg/m^2]	**t** [mm]	**E_{11}** [GPa]	**G_{12}** [GPa]	**ν_{12}** [-]
Fuselage trim panel	255	0.765	3.0	15.0	5.77	0.30
Floor surface panel	1100	3.3	3.0	2.3	0.772	0.49
Overhead bins	100			0.03	0.0125	0.2

Table 8. Biot properties of the floor porous material layer, the fuselage trim melamine acoustic foam and the foam in the seats.

Material	**Density**	**Surface mass**	**Thickness**	**Young's modulus**	**Poisson's ratio**	**Flow resistivity**	**Porosity**	**Tortuosity**	**Loss factor**
	ρ [kg/m^3]	**m** [kg/m^2]	**t** [mm]	**E** [Pa]	**ν** [-]	**σ** [Ns/m^4]	**φ** [-]	**α_∞** [-]	**η** [-]
Melamine foam	8.8	0.704	80	80000	0.4	10900	0.99	1.02	0.17
Floor porous layer	50	2.44	48.8			45000	0.92	1.5	
Seat (foam)	40			95000	0.34	11500	0.95	1.9	0.1

Table 9. LCTR2 cruise flight conditions.

Parameter	Symbol		Outside	Cabin
Operating altitude	h	[m]	8534	2438
Temperature	T	[°C]	-40.7	20.0
Pressure	P	[Pa]	32934	75266
Density	ρ	[kg/m^3]	0.4931	0.897
Speed of sound	c	[m/s]	305.8	343.3
Kinematic viscosity	υ	[m^2/s]	3.05 10^{-5}	2.02 10^{-5}
Heat capacity ratio	γ	[-]	1.401	1.401
Prandtl number	Pr	[-]	0.722	0.715
Free stream flow velocity	U_0	[m/s]	154.3	
Free stream Mach number	M_c	[-]	0.505	

Table 10. Attached turbulent boundary layer thickness as function of distance from the LCTR2 nose.

Fuselage section	Distance from nose [m]	Boundary layer thickness [m]
1	4.24	0.0536
2	5.40	0.0650
3	6.56	0.0760
4	7.72	0.0866
5	8.88	0.0968
6	10.04	0.1068
7	11.20	0.1166
8	12.36	0.1262
9	13.52	0.1356
10	14.68	0.1448
11	15.84	0.1539
12	17.00	0.1628
13	18.16	0.1716
14	19.32	0.1804
15	20.48	0.1890
16	21.64	0.1975
17	22.80	0.2059
18	23.96	0.2143
19	25.12	0.2225

Table 11. Empirical constants used in the Efimtsov turbulent boundary layer model.

a1	a2	a3	a4	a5	a6	a8	a9	a10
0.1	72.8	1.54	0.77	548	13.5	9.55	0.000638	0.00398

Table 12. Boeing 737 flight test conditions.

Parameter	Symbol		Value
Operating altitude	h	[m]	7620
Temperature	T	[°C]	-34.53
Pressure	P	[Pa]	37600
Density	ρ	[kg/m^3]	0.5489
Speed of sound	c	[m/s]	309.7
Kinematic viscosity	υ	[m^2/s]	2.8 10^{-5}
Heat capacity ratio	γ	[-]	1.401
Prandtl number	Pr	[-]	0.72
Free stream flow velocity	U_0	[m/s]	241.5
Free stream Mach number	M_c	[-]	0.78
Distance from the nose	d	[m]	8.81

Table 13. Number of acoustic and structural modes in the one-third octave bands 5–160 Hz.

One-third octave band center frequency [Hz]	Acoustic modes #	Structural modes #
5	1	
6.3		
8		
10		2
12.5	1	2
16	1	4
20		9
25	1	17
31.5	1	19
40	2	29
50	2	31
63	3	42
80	20	73
100	25	93
125	21	129
160	60	183

Table 14. Frequencies of acoustic and structural modes below 20 Hz.

Acoustic mode [Hz]	**Axial mode order**	**Structural mode** [Hz]	**Axial mode order**
5.75	First		
		9.07	First
		9.20	First
11.6	Second	11.4	First
		11.5	First
		14.3	Second
		14.8	Second
		15.3	First
17.6	Third	17.3	Second
		18.5	First
		18.7	Second
		19.4	Third

Table 15. Bombardier Q400 cruise flight conditions.

Parameter	**Symbol**		**Value**
Operating altitude	h	[m]	7620
Temperature	T	[°C]	-34.53
Pressure	P	[Pa]	37600
Density	ρ	[kg/m^3]	0.5489
Speed of sound	c	[m/s]	309.7
Kinematic viscosity	υ	[m^2/s]	2.8 10^{-5}
Heat capacity ratio	γ	[-]	1.401
Prandtl number	Pr	[-]	0.72
Free stream flow velocity	U_0	[m/s]	185.3
Free stream Mach number	M_c	[-]	0.60

FIGURES

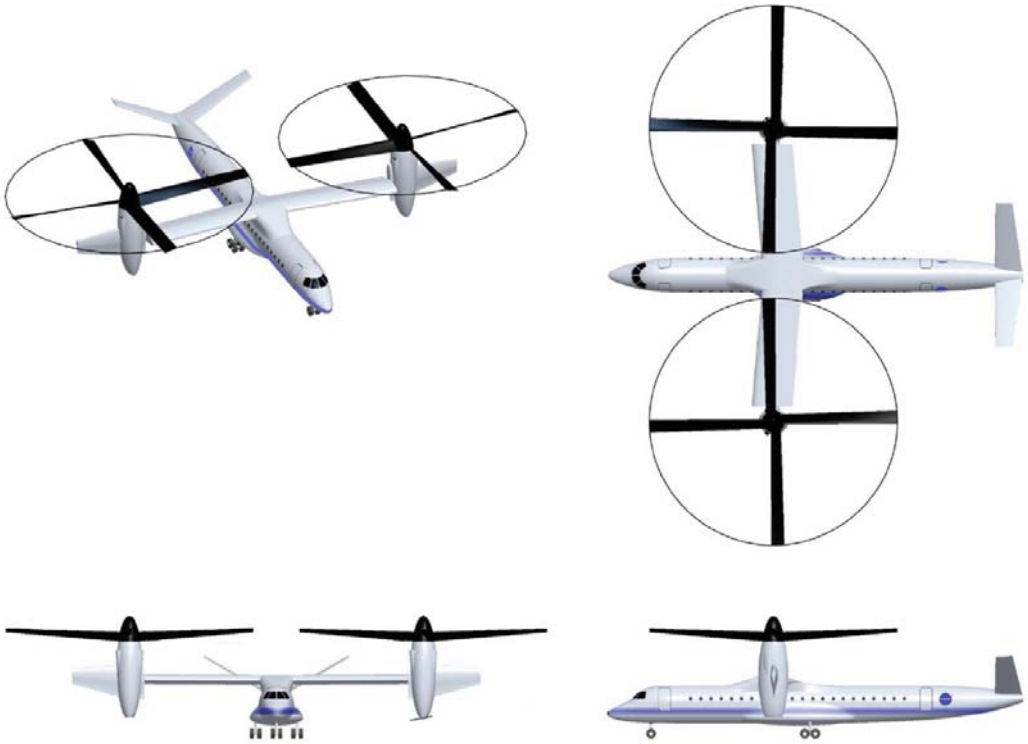

Figure 1. Isometric and three-view of the Large Civil Tiltrotor (LCTR2) design.

Figure 2. Artist's rendering of the LCTR2 concept vehicle in forward flight.

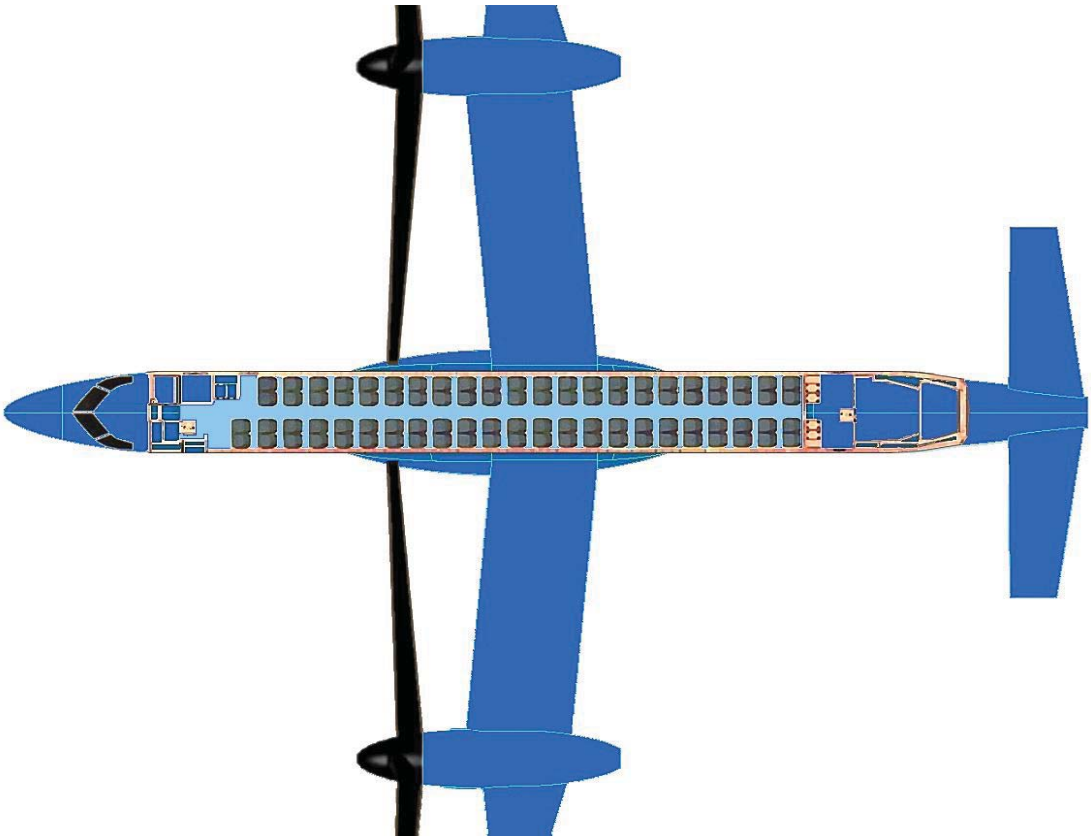

Figure 3. Sketch of a hypothetical LCTR2 90-passenger seating layout.

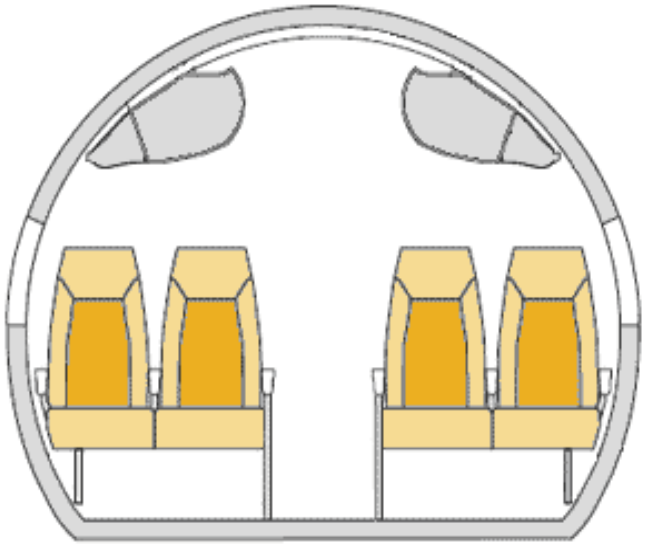

Figure 4. LCTR2 cabin cross-section showing four-abreast seating and overhead bins.

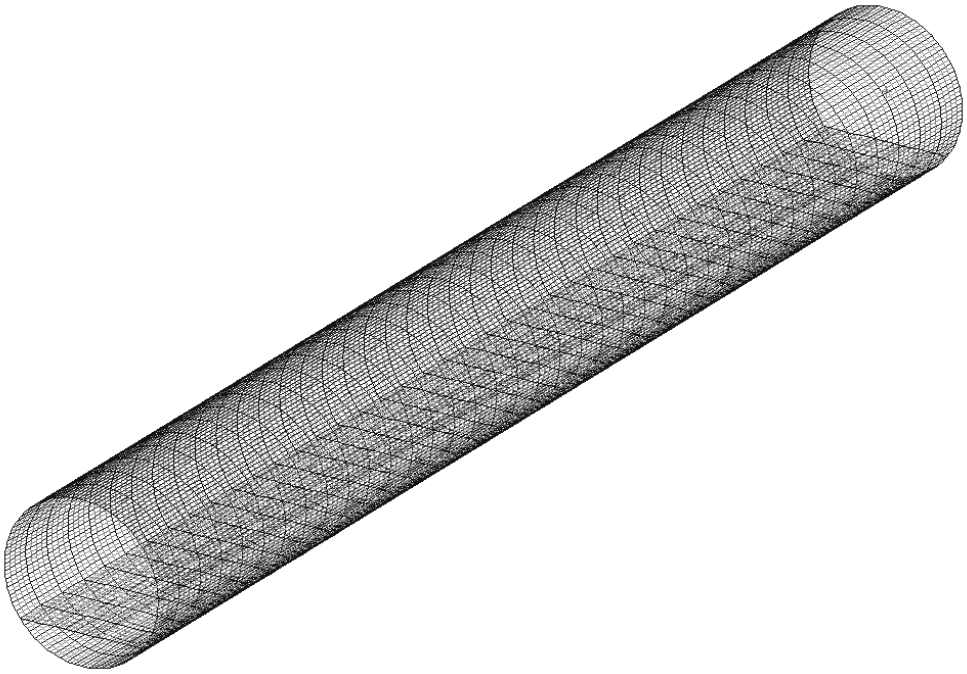

Figure 5. Basic finite element model of the fuselage skin, ring frames, longitudinal stringers, floor, and floor support beams.

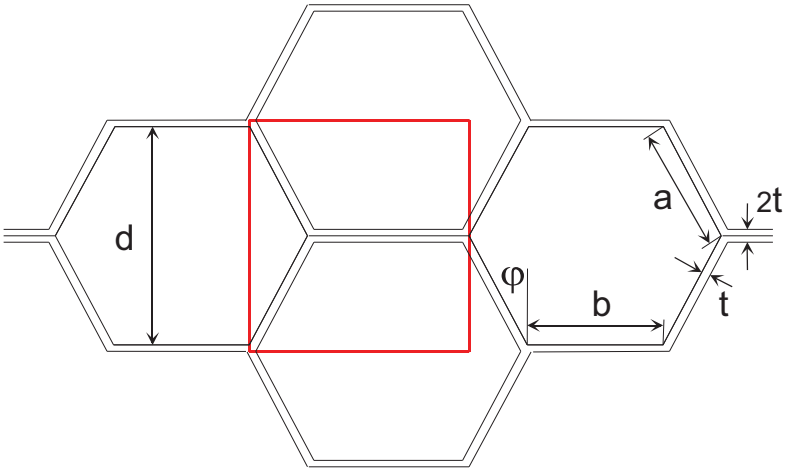

Figure 6. Rectangular unit cell of the honeycomb material.

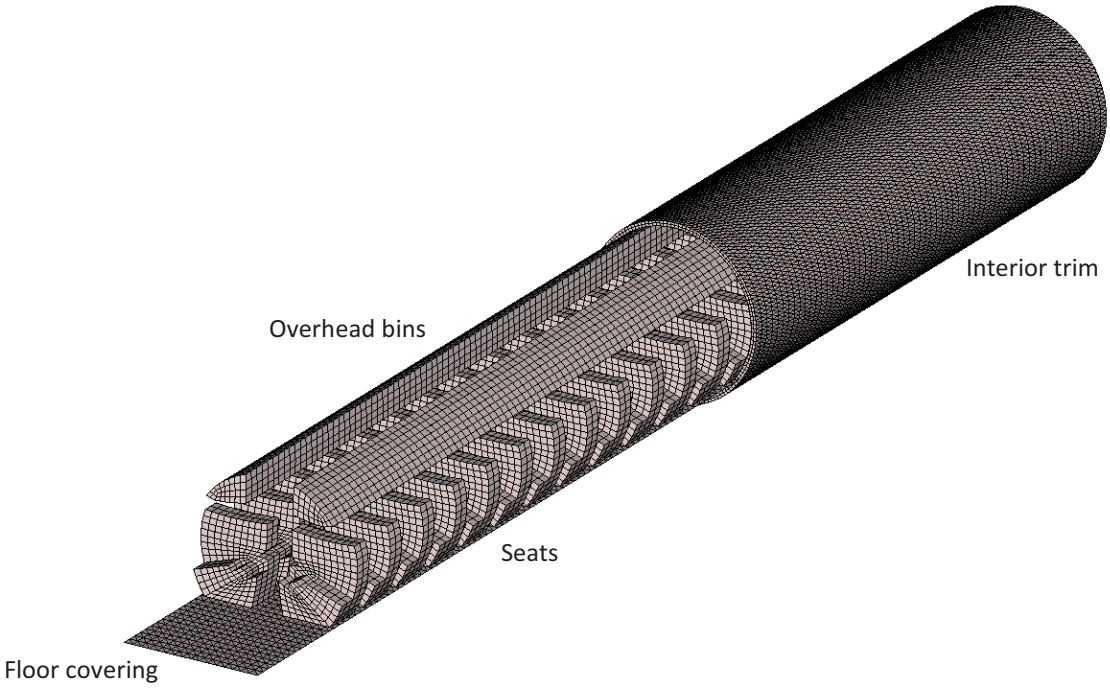

Figure 7. Rudimentary Porous Elastic Finite Element Method (PEM) models for the seats, overhead bins, floor covering and interior trim.

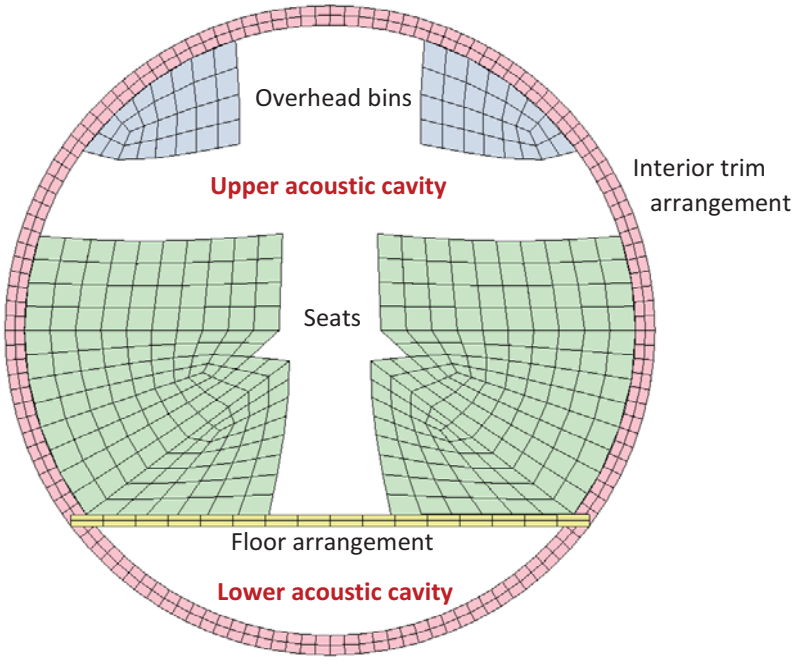

Figure 8. Cross-sectional view of the PEM models for the seats, overhead bins, floor covering and interior trim.

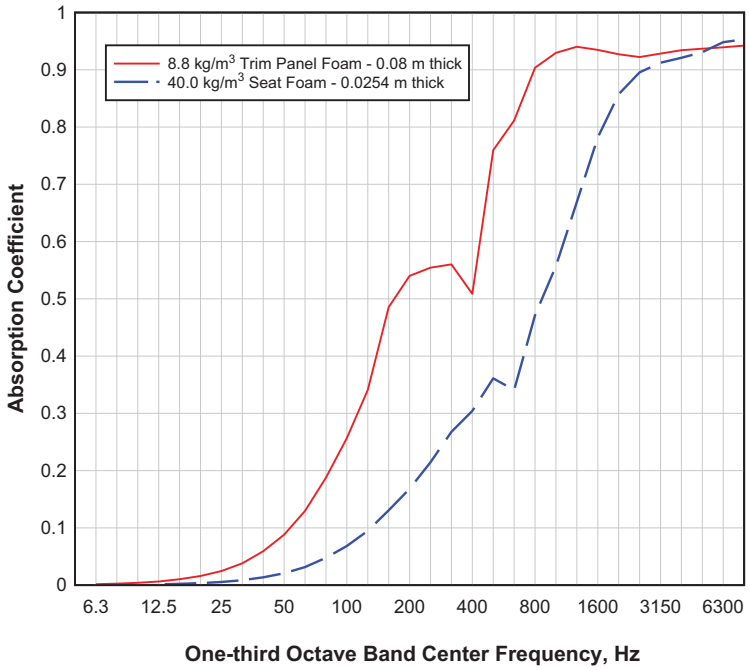

Figure 9. Diffuse field absorption coefficient of 0.08 m thick melamine acoustic foam with a rigid wall boundary condition.

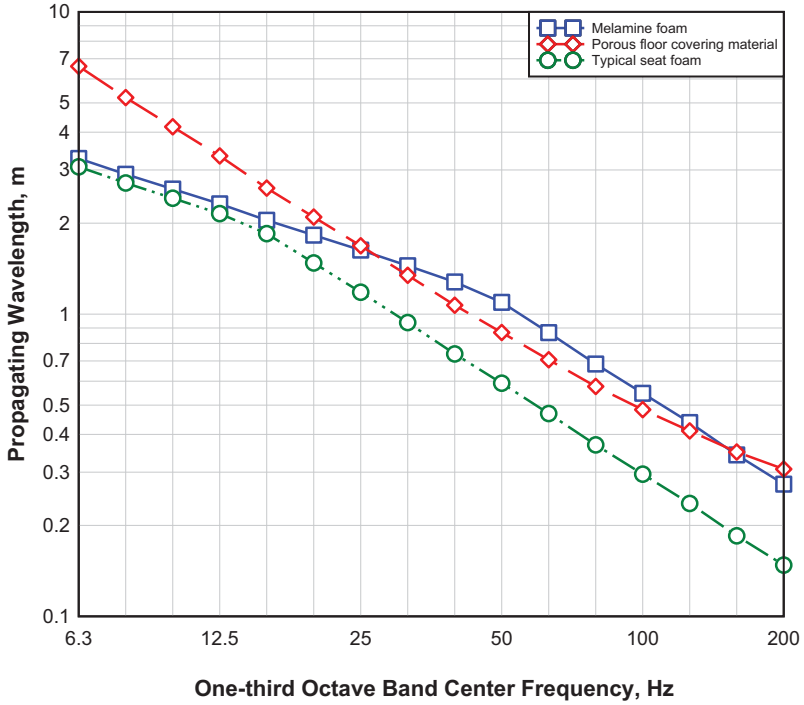

Figure 10. Shortest wavelengths as function of one-third octave band frequency for three poro-elastic materials with the Biot material properties listed in Table 8.

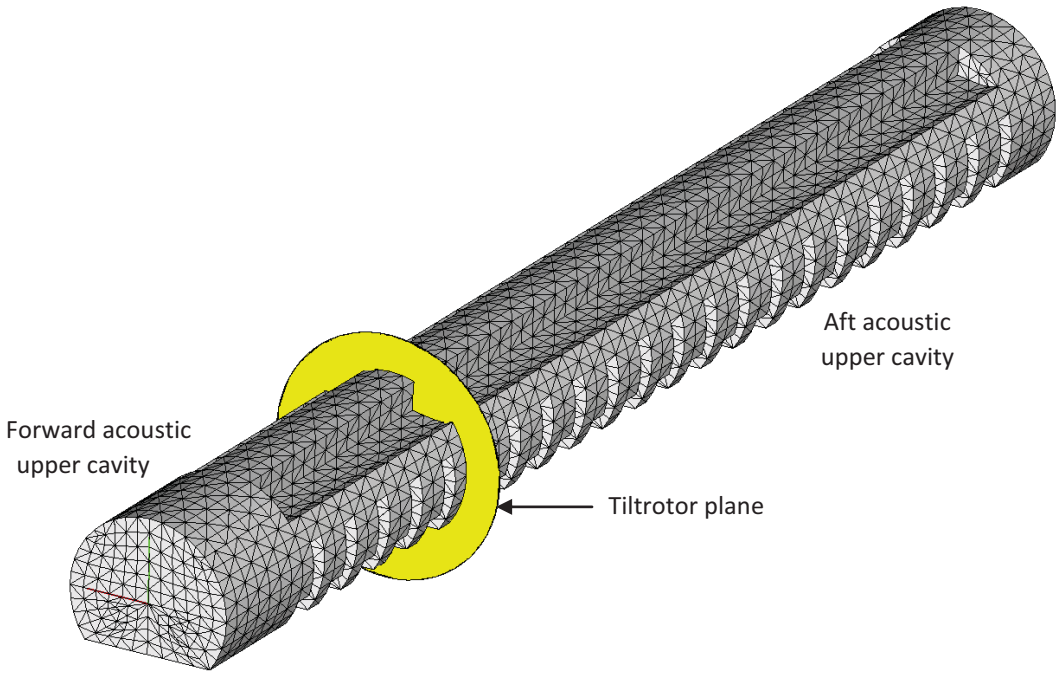

Figure 11. The forward and aft acoustic cavities above the floor relative to the tiltrotor plane.

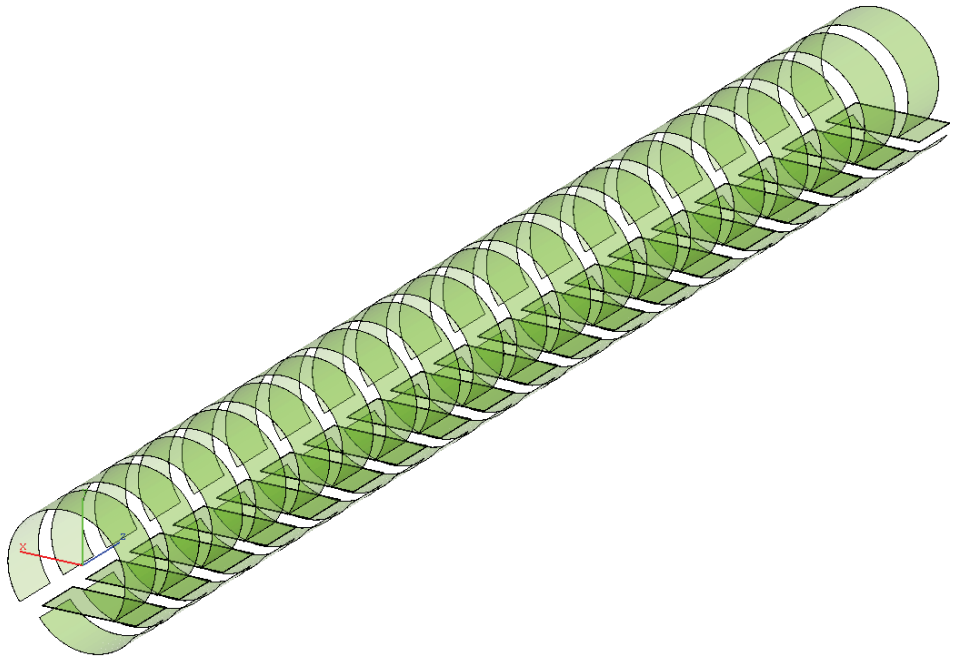

Figure 12. Fifty seven 1.16 m wide structural subsystems (shrunken for clarity), including the floor panels and the curved ribbed skin sections above and below the floor.

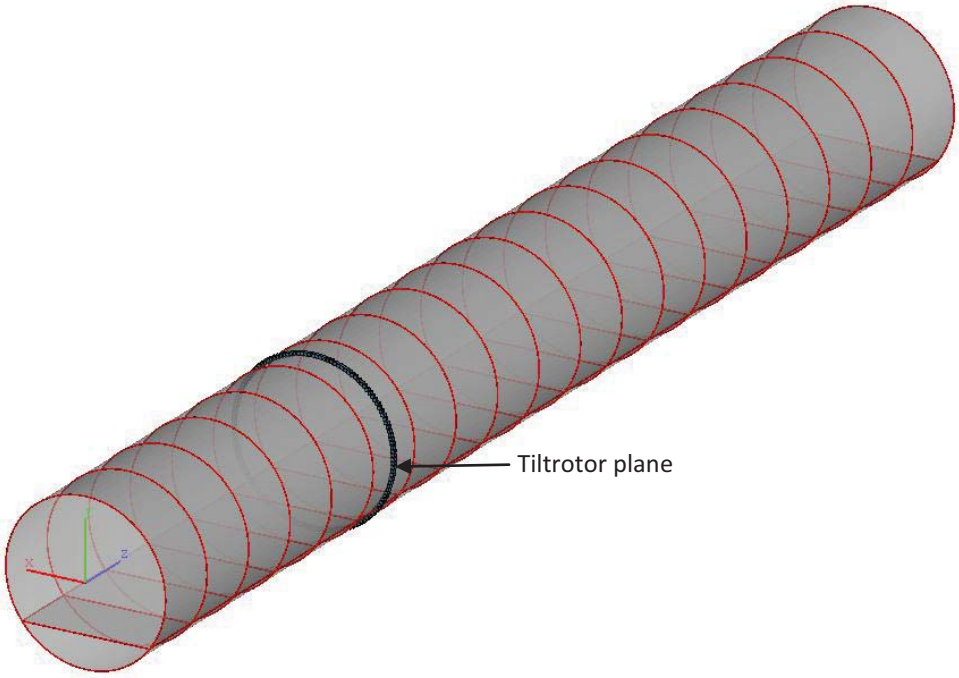

Figure 13. Thirty-eight acoustic cavity sections relative to the tiltrotor plane.

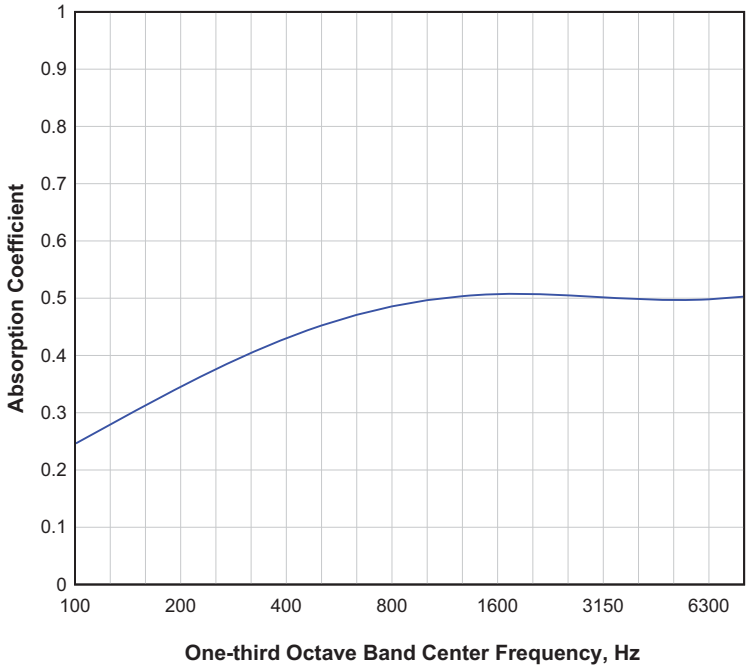

Figure 14. Typical measured average commercial airplane cabin absorption coefficient [15].

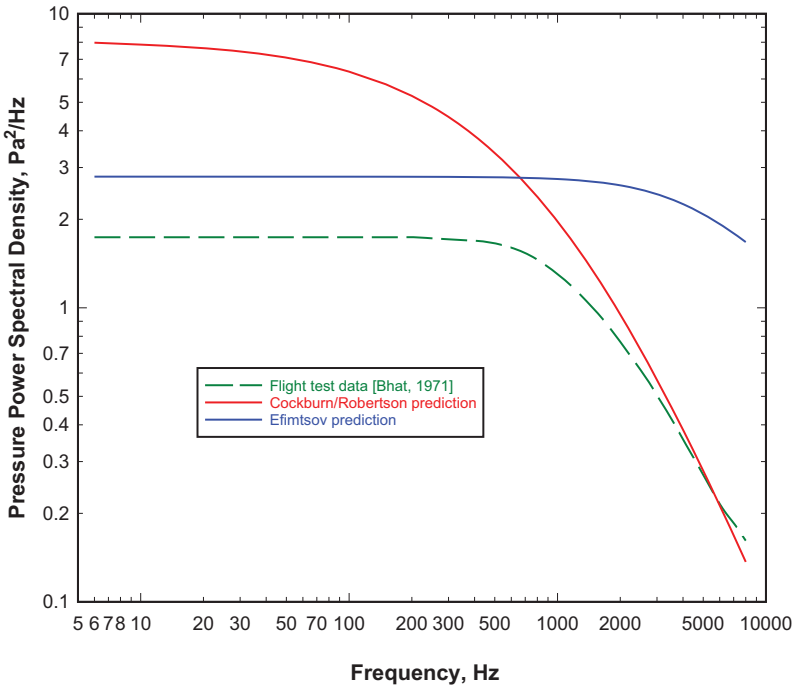

Figure 15. Cockburn/Robertson and Efimtsov predictions compared with flight test measurements of turbulent boundary layer pressure fluctuations on a Boeing 737 aircraft [20].

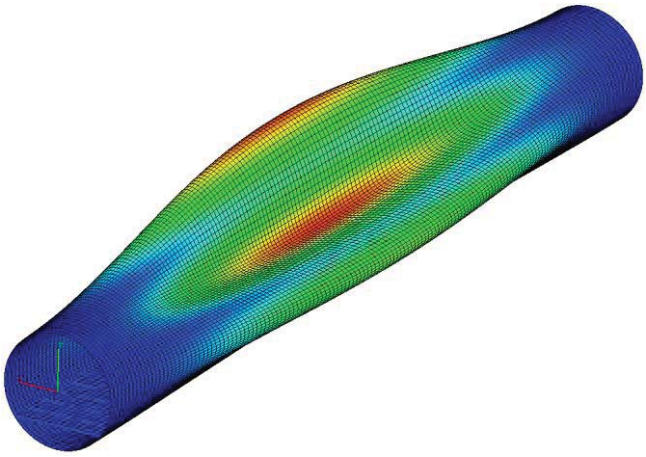

Figure 16. Isometric view of the first structural mode of the fuselage at 9.07 Hz.

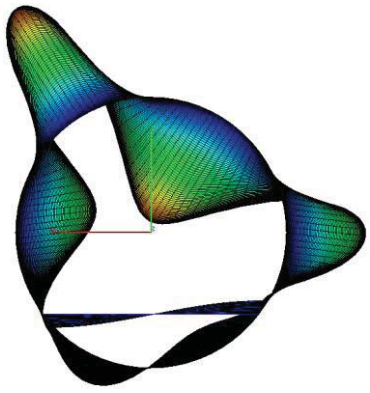

Figure 17. Cross-sectional view of the 9.07 Hz structural fuselage mode.

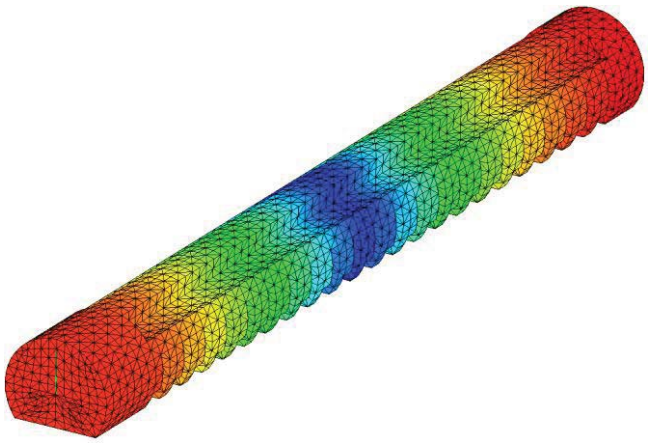

Figure 18. Isometric view of the first acoustic (axial) mode at 5.7 Hz.

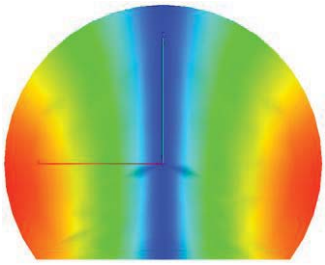

Figure 19. View of the first cross-sectional acoustic mode at 73.8 Hz.

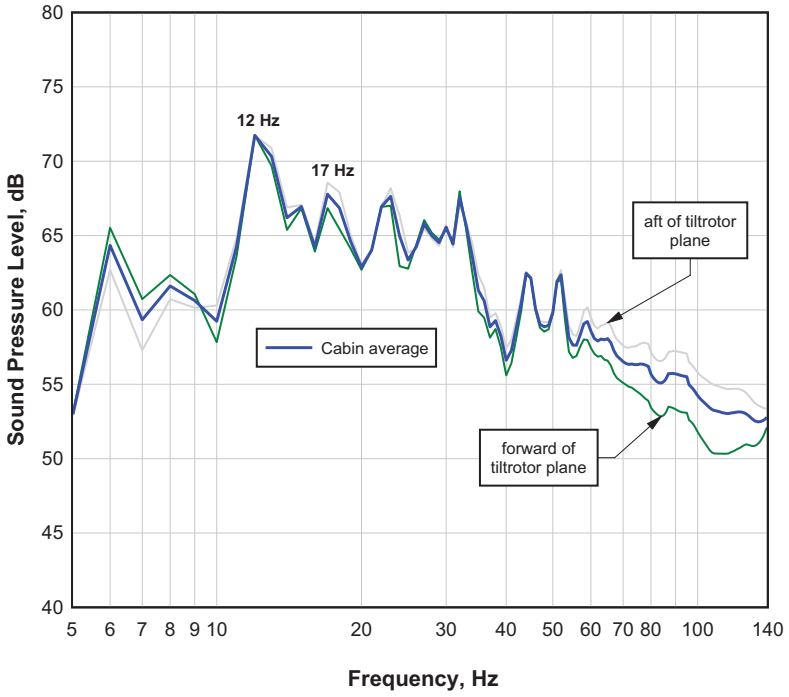

Figure 20. Cabin average of the mean narrowband (1 Hz) LCTR2 cabin sound pressure levels forward and aft of the tiltrotor plane for the Efimtsov boundary layer excitation predicted with the low frequency hybrid FE analysis.

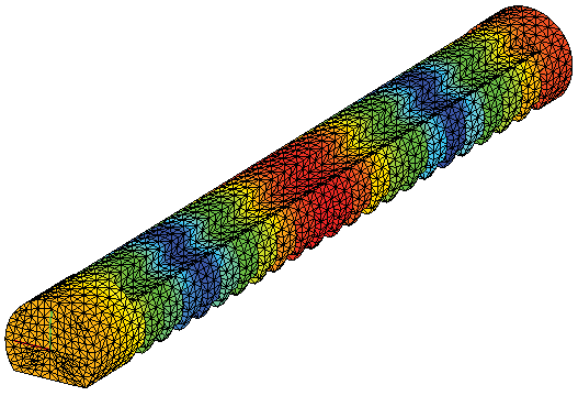

Figure 21. Second-order axial acoustic resonance at 11.6 Hz.

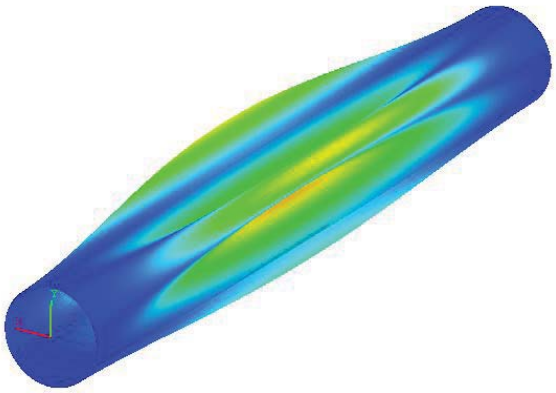

Figure 22. First-order axial structural resonance at 11.3 Hz.

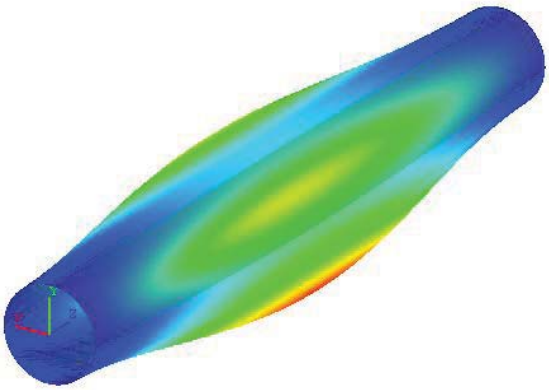

Figure 23. First-order axial structural resonance at 11.5 Hz.

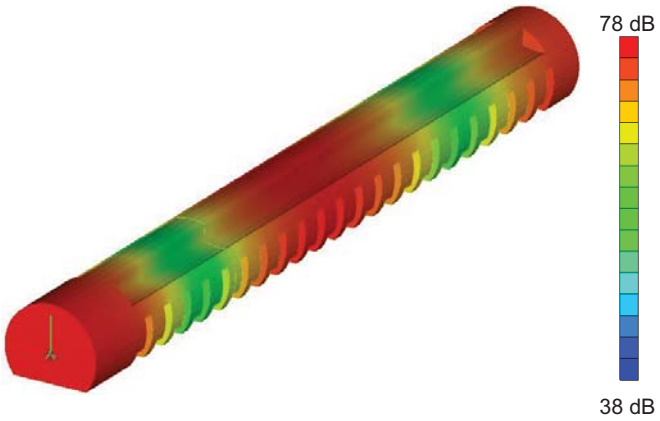

Figure 24. Cabin interior sound pressure level distribution in the 12 Hz band.

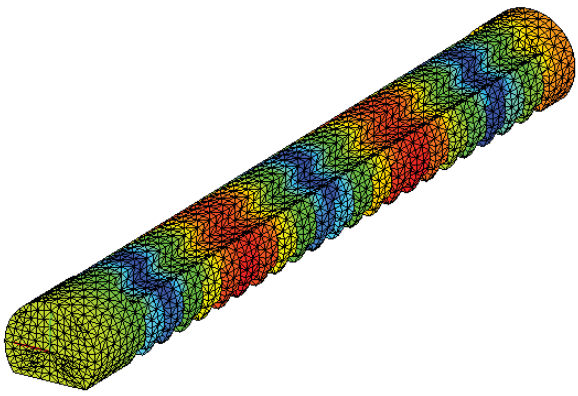

Figure 25. Third-order axial acoustic resonance at 17.6 Hz.

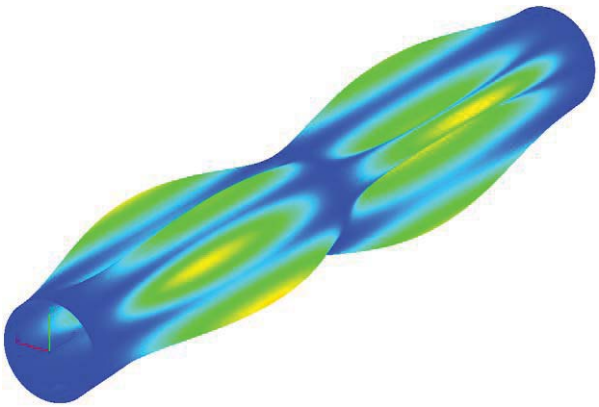

Figure 26. Second-order axial structural resonance at 17.3 Hz.

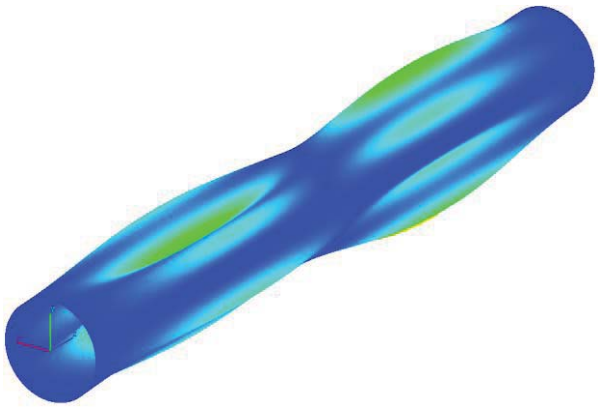

Figure 27. Second-order axial structural resonance at 18.7 Hz.

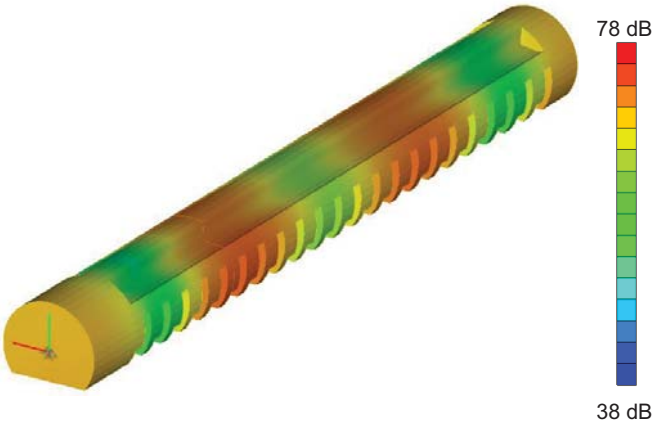

Figure 28. Cabin interior sound pressure level distribution in the 17 Hz band.

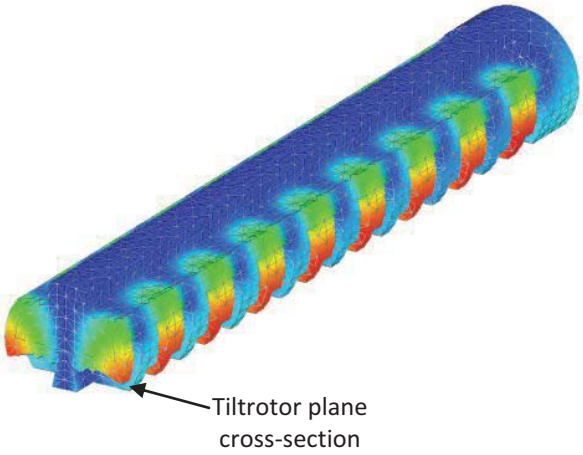

Figure 29. Acoustic resonance (89.2 Hz) with a vertical nodal line in the tiltrotor plane.

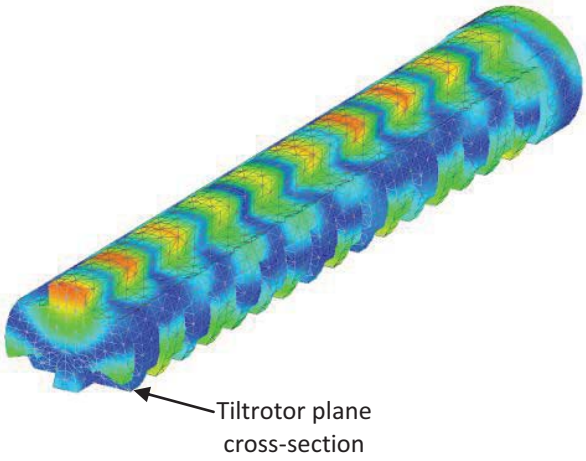

Figure 30. Acoustic resonance (128.9 Hz) with a horizontal nodal line in the tiltrotor plane.

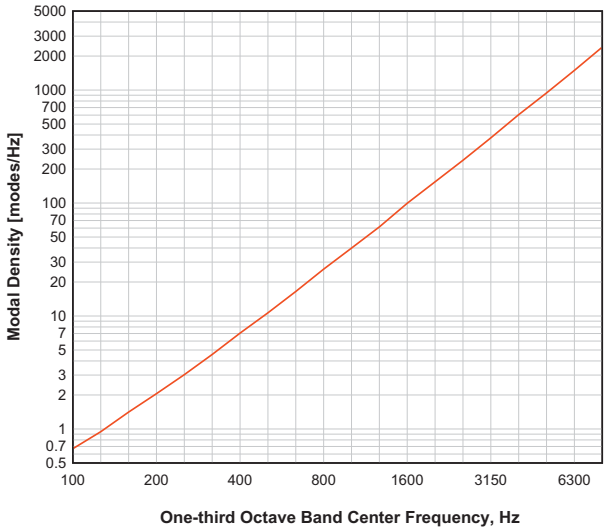

Figure 31. Estimated modal density in the 100 Hz through 8000 Hz one-third octave bands.

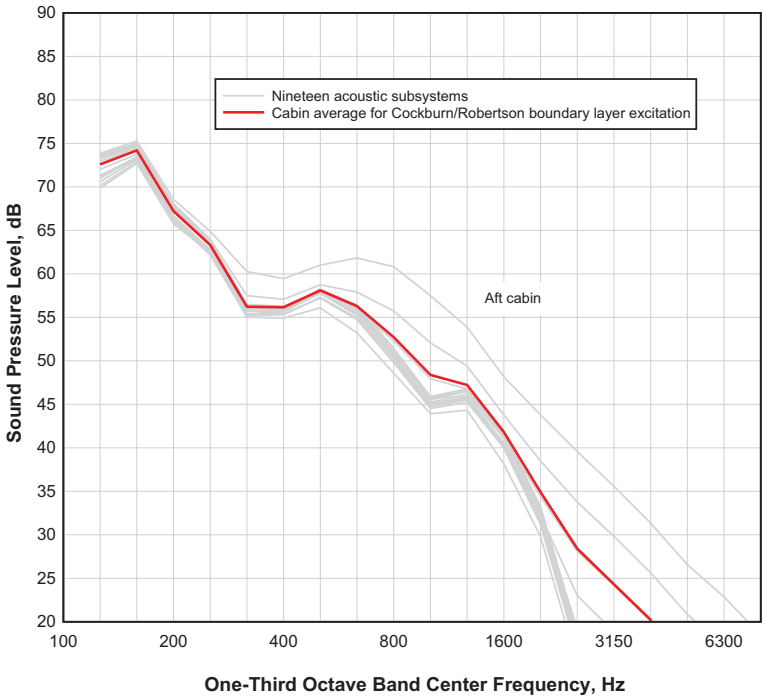

Figure 32. SEA predicted one-third octave band LCTR2 subsystem sound pressure levels and their average for the Cockburn/Robertson turbulent boundary layer excitation.

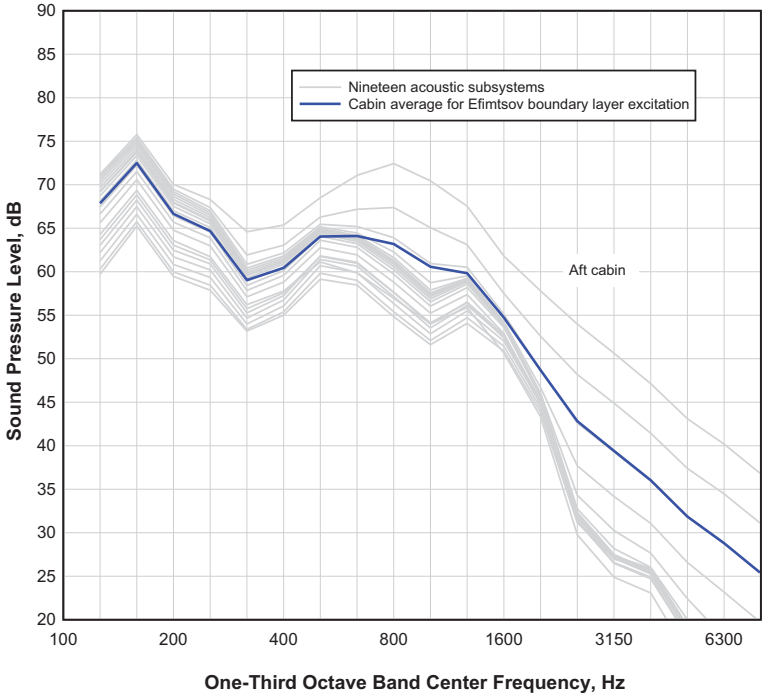

Figure 33. SEA predicted one-third octave band LCTR2 subsystem sound pressure levels and their average for the Efimtsov turbulent boundary layer excitation.

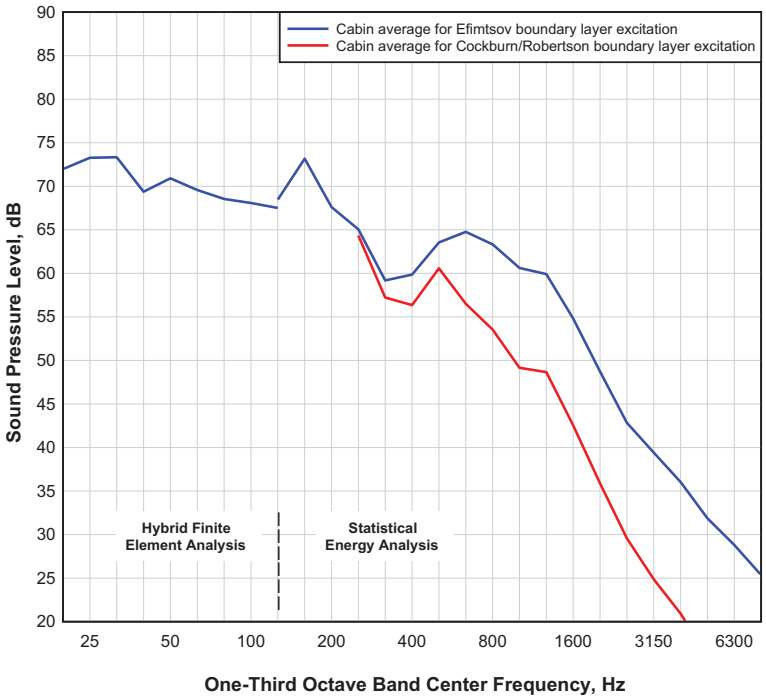

Figure 34. Averaged one-third octave band LCTR2 sound pressure levels predicted with the hybrid FE analysis (20-125 Hz) for the Efimtsov boundary layer excitation, and with SEA (125-8000 Hz) for both the Efimtsov and Cockburn Robinson models.

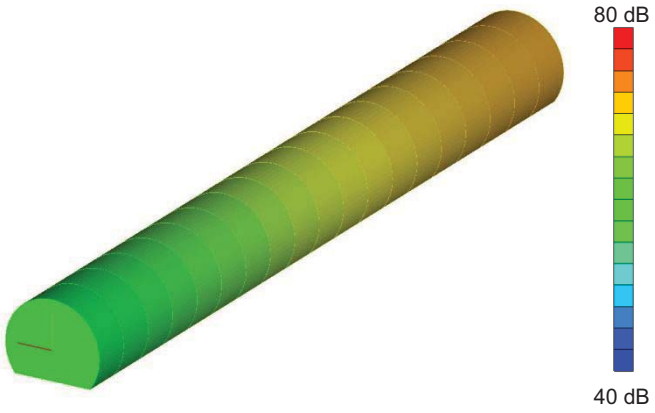

Figure 35. SEA predicted cabin interior sound pressure levels in the 125 Hz one-third octave band due to Efimstov turbulent boundary layer excitation.

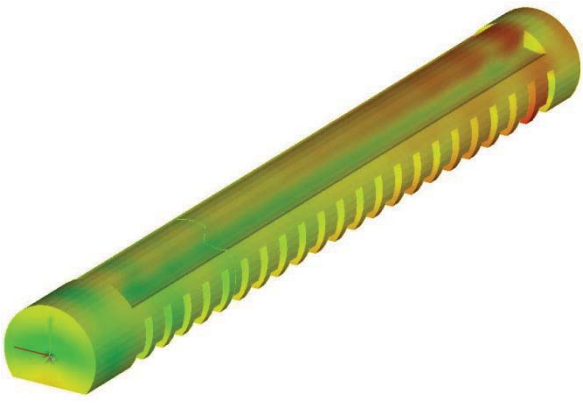

Figure 36. FE predicted cabin interior sound pressure levels in the 125 Hz one-third octave band due to Efimstov turbulent boundary layer excitation.

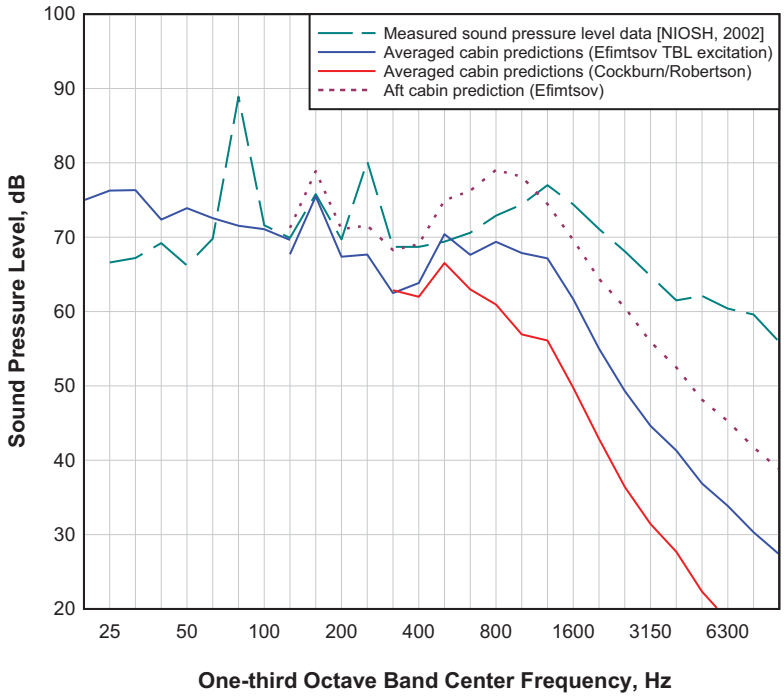

Figure 37. Averaged predicted LCTR2 one-third octave band sound pressure levels compared to measurements in the Bombardier Q400 aircraft.

REPORT DOCUMENTATION PAGE

Form Approved
OMB No. 0704-0188

1. REPORT DATE *(DD-MM-YYYY)*	2. REPORT TYPE	3. DATES COVERED *(From - To)*
01- 06 - 2013	Contractor Report	

4. TITLE AND SUBTITLE

Large Civil Tiltrotor (LCTR2) Interior Noise Predictions Due to Turbulent Boundary Layer Excitation

5a. CONTRACT NUMBER
NNL12AA09C

5b. GRANT NUMBER

5c. PROGRAM ELEMENT NUMBER

6. AUTHOR(S)

Grosveld, Ferdinand W.

5d. PROJECT NUMBER

5e. TASK NUMBER

5f. WORK UNIT NUMBER
380046.02.07.04.01.05

7. PERFORMING ORGANIZATION NAME(S) AND ADDRESS(ES)
NASA Langley Research Center
Hampton, Virginia 23681

8. PERFORMING ORGANIZATION REPORT NUMBER

9. SPONSORING/MONITORING AGENCY NAME(S) AND ADDRESS(ES)
National Aeronautics and Space Administration
Washington, DC 20546-0001

10. SPONSOR/MONITOR'S ACRONYM(S)
NASA

11. SPONSOR/MONITOR'S REPORT NUMBER(S)
NASA/CR-2013-218005

12. DISTRIBUTION/AVAILABILITY STATEMENT
Unclassified - Unlimited
Subject Category 71
Availability: NASA CASI (443) 757-5802

13. SUPPLEMENTARY NOTES
This report was prepared by Northrop Grumman under NASA contract NNL12AA09C with Analytical Mechanics Associates, Inc., Hampton, VA
Langley Technical Monitor: Randolph H. Cabell

14. ABSTRACT

The Large Civil Tiltrotor (LCTR2) is a conceptual vehicle that has a design goal to transport 90 passengers over a distance of 1800 km at a speed of 556 km/hr. In this study noise predictions were made in the notional LCTR2 cabin due to Cockburn/Robertson and Efimtsov turbulent boundary layer (TBL) excitation models. A narrowband hybrid Finite Element (FE) analysis was performed for the low frequencies (6-141 Hz) and a Statistical Energy Analysis (SEA) was conducted for the high frequency one-third octave bands (125-8000 Hz). It is shown that the interior sound pressure level distribution in the low frequencies is governed by interactions between individual structural and acoustic modes. The spatially averaged predicted interior sound pressure levels for the low frequency hybrid FE and the high frequency SEA analyses, due to the Efimtsov turbulent boundary layer excitation, were within 1 dB in the common 125 Hz one-third octave band. The averaged interior noise levels for the LCTR2 cabin were predicted lower than the levels in a comparable Bombardier Q400 aircraft cabin during cruise flight due to the higher cruise altitude and lower Mach number of the LCTR2. LCTR2 cabin noise due to TBL excitation during cruise flight was found not unacceptable for crew or passengers when predictions were compared to an acoustic survey on a Q400 aircraft.

15. SUBJECT TERMS

Acoustics; Finite element; Interior noise; Noise prediction; Tiltrotor; Turbulent boundary layer

16. SECURITY CLASSIFICATION OF:			17. LIMITATION OF ABSTRACT	18. NUMBER OF PAGES	19a. NAME OF RESPONSIBLE PERSON
a. REPORT	b. ABSTRACT	c. THIS PAGE			STI Help Desk (email: help@sti.nasa.gov)
					19b. TELEPHONE NUMBER *(Include area code)*
U	U	U	UU	42	(443) 757-5802